Korean J. Chem. Eng., 37(8), 1275-1294 (2020)
DOI: 10.1007/s11814-020-0626-y

pISSN: 0256-1115
eISSN: 1975-7220

INVITED REVIEW PAPER

Electrodeposition-fabricated catalysts for polymer electrolyte water electrolysis

Hoyoung Kim‡, Hyanjoo Park‡, Hotae Bang, and Soo-Kil Kim†

School of Integrative Engineering, Chung-Ang University, 84 Heukseok-ro, Dongjak-gu, Seoul 06974, Korea
(*Received 28 March 2020 • Revised 5 June 2020 • Accepted 7 July 2020*)

Abstract−Water electrolysis using renewable energy sources such as solar and wind power has the advantage of producing hydrogen with high efficiency and zero emissions. Solid polymer electrolyte water electrolysis (SPEWE) is divided into anion exchange membrane electrolysis (AEMWE) carried out in an alkaline environment and proton exchange membrane electrolysis (PEMWE) carried out in an acidic environment. Research on the electrocatalysts used in these electrolysis procedures has focused on the development of transition metal-based catalysts with catalytic activity, high stability, and low cost that can replace the currently used noble-metal based electrocatalysts. Among the various electrocatalyst fabrication methods, electrodeposition can be used to fabricate catalysts in a simple manner at low cost and high purity. In addition, catalysts can be directly electrodeposited onto a substrate such as a gas diffusion layer, simplifying the electrode fabrication process and readily enabling the advantageous control of the physical, chemical, structural, and compositional properties of the catalyst. In this paper, we summarize the characteristics and structures of the water electrolysis catalysts prepared by the electrodeposition method based on recent research studies that suggest their applicability to practical water electrolysis systems in the future.

Keywords: Electrodeposition, Electrocatalysts, Water Electrolysis, Hydrogen Evolution, Oxygen Evolution

INTRODUCTION

Depending on the electrolyte type and operating temperature, water electrolysis processes for the production of high-purity hydrogen used as a clean energy source are generally classified into three categories: solid oxide electrolysis, alkaline electrolysis, and proton exchange membrane electrolysis [1-7]. Fig. 1 illustrates these three processes and their operating principles [1-4]. Solid oxide electrolysis (Fig. 1(a)) uses an oxide film, such as zirconia having oxide ion conductivity as an electrolyte and a separator, and operates at a high temperature of 700 to 900 °C [3-6]. Although it has faster kinetics (thus possible use of non-noble catalyst) and lower electrical energy consumption due to its high operation temperatures, it is still in the early stage of development, having many issues to overcome including durability. Secondly, alkaline electrolysis (Fig. 1(b)) using an alkali electrolyte such as 20-40% NaOH or KOH is currently the most widely commercialized method because of the simple structure of the electrolysis device and its low manufacturing cost due to the use of a non-noble metal catalyst [1,2,8-12]. However, this approach needs electrolyte replenishment to maintain the concentration of the electrolyte solution, has corrosion by the alkaline electrolyte solution, low current density and efficiency, and crossover of the gas through the diaphragm [1,2,8-12]. To overcome the disadvantages of the diaphragms used in alkaline electrolyzers, proton exchange membrane water electrolysis (PEMWE, Fig. 1(c)) using a solid sulfonated polymer membrane that conducts protons as an electrolyte has been studied [1,13-15]. PEMs such as Nafion® and Fumapem® can achieve high currents by reducing ohmic loss because of their low film thickness (~20-300 μm) and high proton conductivity [1-3,16-18]. These PEMs also exhibit low gas crossover, enabling the production of hydrogen with high purity. However, because protons are used as charge transfer ions, these systems must operate in harsh corrosive acidic environments, necessitating the use of expensive Pt-group metals (PGMs) with high corrosion resistance as catalysts or Ti-based materials as the current collector and separator plate [1-3,5].

In addition to the above-mentioned alkaline electrolysis and PEMWE, the development of anion exchange membrane water electrolysis (AEMWE) has recently been investigated. Unlike alkaline electrolysis, AEMWE adopts AEM as an electrolyte instead of the diaphragm-separated concentrated KOH or NaOH. The use of distilled water or a low-concentration alkaline solution as the water feed mitigates the issues of corrosion and gas crossover, and the use of the AEM that is less expensive than PEM and of the non-noble catalysts also lowers the cost of hydrogen production [7,19,20].

As described above, water electrolysis is mainly performed in a strong basic or acidic solution, where the reactions at both electrodes can be described as follows [1-7].

In alkaline solution: $2H_2O\ (l)+2e^- \rightarrow H_2\ (g)+2OH^-\ (aq)$
(cathode, E^0_{red}=−0.83 V vs. NHE)
$2OH^-\ (aq) \rightarrow H_2O\ (l)+1/2O_2\ (g)+2e^-$
(anode, E^0_{ox}=0.40 V vs. NHE)

In acidic solution: $2H^+\ (aq)+2e^- \rightarrow H_2\ (g)$
(cathode, E^0_{red}=0.00 V vs. NHE)
$H_2O\ (l) \rightarrow 2H^+\ (aq)+1/2O_2\ (g)+2e^-$
(anode, E^0_{ox}=1.23 V vs. NHE)

Total reaction: $H_2O\ (l) \rightarrow H_2\ (g)+1/2O_2\ (g)$ (E^0_{cell}=−1.23 V)

Theoretically, water electrolysis requires an energy input of ap-

†To whom correspondence should be addressed.
E-mail: sookilkim@cau.ac.kr
‡Equally contributed.

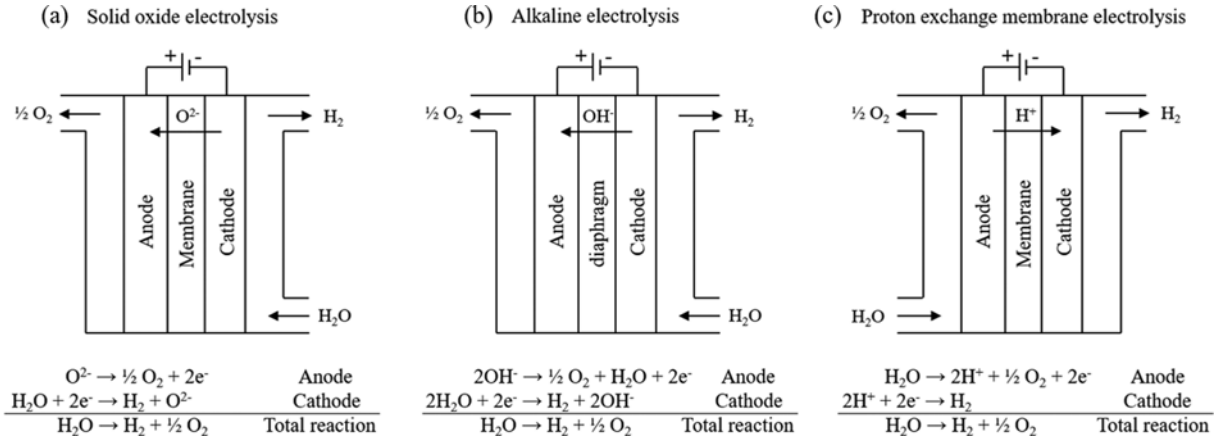

Fig. 1. Schematic and overall reactions of the (a) solid oxide, (b) alkaline, and (c) proton exchange membrane electrolysis systems (Redrawn from Ref. [1-4]).

proximately 1.23 V, but the overpotential resulting from the polarization at the electrodes, ohmic compartments, and mass transport phenomena requires the use of a higher potential, reducing the energy efficiency of hydrogen production. Particularly for the kinetic overpotential, the use of an electrochemical catalyst is essential to improve both the hydrogen evolution reaction (HER) and oxygen evolution reaction (OER), regardless of the electrolyte types. To date, it has been shown that Pt-based catalysts [1,18,21-27] and Ir or Ru-based catalysts [1,2,5,28-32] exhibit high activity in HER and OER, respectively. However, because of the high cost and scarcity of these noble metal catalysts, research for the development of transition-metal-based catalysts with high efficiency/durability has attracted much attention. For alkaline water electrolysis, transition metals and their alloys of Ni [8,33-48], Cu [49-57], and Co [58-70] have been frequently investigated. For acidic OER, the use of noble metals is unavoidable because they operate in a range of significant positive potential in a corrosive electrochemical environment [1,2,5,28-32]. However, for HER, it is possible to use a non-PGM catalyst because HER is carried out at a relatively negative potential [71-93]. Therefore, it is important to understand the reaction mechanism of HER and OER and to design catalysts that can function properly under different conditions.

The HER process in hydrogen production consists of three steps in alkaline [94-96] and acidic [94,97,98] media:

Volmer reaction: $H_2O+M+e^- \rightarrow M\text{-}H_{ads}+OH^-$ (alkaline medium)
$H^+ + M + e^- \rightarrow M\text{-}H_{ads}$ (acidic medium)
Heyrovsky reaction: $M\text{-}H_{ads}+H_2O+e^- \rightarrow M+OH^-+H_2$ (alkaline medium)
$M\text{-}H_{ads}+H^+ + e^- \rightarrow M+H_2$ (acidic medium)
Tafel reaction: $2M\text{-}H_{ads} \rightarrow 2M+H_2$

The water and protons in the electrolyte are reduced at the catalyst surface through a Volmer reaction and form adsorbed hydrogen atoms on the catalyst surface. Subsequently, hydrogen is generated either by the Heyrovsky reaction in which the adsorbed hydrogen atoms react with water or protons, or by the Tafel reaction in which the adsorbed hydrogen atoms combine with each other. Therefore, to obtain high catalytic activity in HER, the catalyst must have a moderate bond strength to hydrogen that are neither too strong nor too weak. Based on this principle, almost all transition metals and their alloys/compounds have been screened for HER activity both in alkaline [34,35,37,38,40,43-48,52,54,57,58,61,62-66,68,69] and acidic [71-93] environments. Among these, Ni is one of the most intensely studied catalysts because of its low cost and high chemical stability and its moderate hydrogen bond strength [99,100].

The mechanism of the OER on metal and oxide surfaces is known to be more complicated than the HER mechanism [101-103]. To date, the OER mechanisms in alkaline and acidic media have not been completely understood. However, among the various proposed OER mechanisms [104-109], the generally accepted mechanism is strongly dependent on the pH of the medium and involves the production of reaction intermediates such as M-O and M-OH, with two different reactions proceeding from the M-O intermediate to O_2 evolution. Examples of these mechanisms are as follows [101,109].

Alkaline medium: $M+OH^- \rightarrow M\text{-}OH_{ads}+e^-$
$M\text{-}OH_{ads}+OH^- \rightarrow M\text{-}O_{ads}+H_2O+e^-$
$2M\text{-}O_{ads} \rightarrow 2M+O_2$
$M\text{-}O_{ads}+OH^- \rightarrow M\text{-}OOH_{ads}+e^-$
$M\text{-}OOH_{ads}+OH^- \rightarrow M+O_2+H_2O+e^-$
Acidic medium: $M+H_2O \rightarrow M\text{-}OH_{ads}+H^++e^-$
$M\text{-}OH_{ads} \rightarrow M\text{-}O_{ads}+H^++e^-$
$2M\text{-}O_{ads} \rightarrow 2M+O_2$
$M\text{-}O_{ads}+H_2O \rightarrow M\text{-}OOH_{ads}+H^++e^-$
$M\text{-}OOH_{ads} \rightarrow M+O_2+H^++e^-$

As shown in the above reaction pathway, when the OH^- or H_2O molecules are bound to the catalyst surface, O_2 is produced by two pathways depending on the pH of the medium. Theoretically, OER is initiated by the adsorption of OH^- ions on the active site of the catalyst, and the use of suitable catalysts with an appropriate affinity for the OH intermediates is known to promote their formation and equilibrium coverage, resulting in high OER activity [110]. However, designing OER catalysts is difficult because of the sluggish four-electron transfer process in the water oxidation process [111].

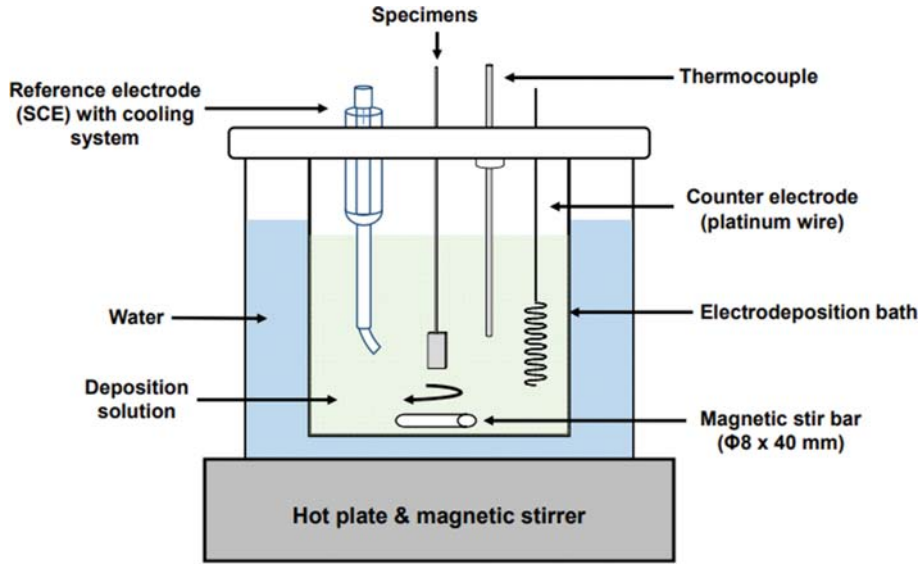

Fig. 2. Schematic of an example of the electrodeposition apparatus (Reproduced from Ref. [116]). This is a typical 3-electrode batch type system consisting of a reference electrode, a counter electrode, and a working electrode. The bath temperature can be controlled by an external water jacket combined with a hot plate. The mass transport of the reactants can be adjusted either by magnetic stirring or a rotation disk electrode (not shown here).

Moreover, even oxide catalysts with the same composition have been found to exhibit different electro-kinetic profiles depending on the fabrication method and the structure of the oxide layer, giving rise to different activities [30,31,112-115]. Even though very good OER activity has been obtained using oxides of noble metals such as RuO_2 and IrO_2 in acidic media, the use of these noble metal catalysts is not economically viable because of their high cost and scarcity [1,2,5,28-32]. Therefore, an intense research effort is underway to develop inexpensive and efficient OER catalysts based on nitrides, oxides, and phosphides to replace these noble metal catalysts.

Electrodeposition is a universal method for the preparation of catalysts using a simple process, at relatively low cost, and with high purity compared to chemical synthesis. Fig. 2 shows a schematic of an example of the electrodeposition process [116]. Various physico-chemical properties such as particle shape, composition, and crystallinity can be controlled simply by adjusting the electrodeposition parameters such as precursor composition, deposition potential/current, and time [39,79,92,117-138]. In addition, catalysts can be easily electrodeposited onto the substrate at room temperature and ambient pressure conditions, enabling one-pot production of catalyst-coated substrate (CCS) gas diffusion electrode for the electrolytic and fuel cell system [79,92,124,129,130,132-134]. Direct electrodeposition of thin catalyst layer on the carbon or titanium fibers constituting the gas diffusion layer (GDL) enables the catalyst layer to have similar macro pore structures to that of the GDL, which facilitates the mass transport of the reactants and the products. In contrast, coating of synthetically prepared catalysts on the GDL or membrane generally requires multiple steps and binder/ionomer containing ink solution. Spray coating or brushing of the catalyst ink solution often results in the non-uniform coating of thick and dense catalyst layer, where the control of pore structures is a critical issue. In addition, the use of binder/ionomer is not always necessary for the electrodeposited catalyst layer, particularly for the water electrolysis system. This is because i) the formation of the catalyst particle is preferentially occurring on the surface of conducting substrate giving good adhesion [139,140], and ii) the liquid water can effectively deliver protons or hydroxide ions within the catalyst layer. In addition, the absence of polymer binders leads to hydrophilic conditions throughout the catalyst layer, which is beneficial to the transport of ions by water and release of produced bubbles. Therefore, the electrochemical deposition method, which can be used to form a stable electronic/physical contact between the catalyst and the gas diffusion layer, is a suitable strategy for easily improving the structural characteristics important for gas transport, providing improved electrochemically active areas, and excellent catalytic activity/durability during the electrochemical energy conversion processes.

ALKALINE WATER ELECTROLYSIS

1. Oxygen Evolution Reaction (OER)

OER is the anodic reaction of water electrolysis that requires a larger overpotential than HER and is thus the bottleneck of the water electrolysis reaction. To reduce the OER overpotential and further improve the overall reaction rate, it is necessary to develop an appropriate catalyst. Although oxides of noble metals such as IrO_2 and RuO_2 have been used as OER catalysts, the high price and scarcity of noble metals have motivated a research effort to develop non-noble metal-based catalysts with high catalytic activity and high stability for alkaline OER for practical application [5]. Therefore, investigations aiming to increase the catalyst activity and stability of inexpensive transition-metal materials such as metal nitrides, oxides, phosphides, and chalcogenides are ongoing. Accordingly,

the recent trends in the studies on the electrodeposition-fabricated alkaline OER catalysts are introduced below based on the key transition metal of the catalyst.

1-1. Ni-based Electrocatalysts

Ni-based catalysts are generally used as anode materials as well as cathode materials in alkaline media, but pure Ni metal has low activity and stability against water splitting. Therefore, many studies have been conducted to reduce the overpotential through alloying with other transition metals and non-metal elements. Table 1 summarizes the OER activities of Ni-based alloy/compound catalysts prepared by electrodeposition [33-42]. In a representative study, Luo et al. reported NiFe nanosheet films (NiFe/NF) on Ni foams by one-step electrodeposition to measure the OER and HER activity and durability in 1.0 M KOH electrolyte [34]. It was found that the OER had an overpotential of 264 mV at 20 mA cm^{-2} and Tafel slope of 51 mV dec^{-1}, while an overpotential of 139 mV at 10 mA cm^{-2} and Tafel slope of 112 mV dec^{-1} were obtained for HER. In addition, a stability test carried out for 500 cycles for both OER and HER showed excellent stability of the catalyst activity compared to that in the first cycle. Pu et al. prepared $NiSe_2$/Ti electrode by electrodeposition [35]. They reported that these catalysts acted as conducting support to provide electron paths for the NiOOH active species during OER, exhibiting excellent OER activity with an overpotential of 295 mV at 20 mA cm^{-2} and Tafel slope of 82 mV

Table 1. Summary of the alkaline OER performance for Ni-based catalysts

Catalyst	Deposition condition			Heat treatment	Electrolyte	Tafel slope (mV dec^{-1})	Overpotential (mV)			Exchange current density (mA cm^{-2})	Ref.
	Electrolyte	Potential/Current/ Time	Temp. (°C)				η_{10}	η_{20}	η_{100}		
Ni nanocones array (NNA)/ NF	1.0 M $NiCl_2{\cdot}6H_2O$+3 M NH_4Cl+2 M ammonia	–60 mA for 150 s	50		1.0 M KOH	96	345				[33]
NiFe-OH@NNA/ NF	0.4 mM $FeCl_3{\cdot}6H_2O$+ 2.49 mM $NaNO_3$	(immersion for 5 s)	100			53	316				
NiFe/NF	0.2 M $NiSO_4{\cdot}7H_2O$+ 0.2 M $FeSO_4{\cdot}7H_2O$	CV: –0.2~–1.4 V_{SCE}, scan rate of 50 mV/s, for 60 cycles	RT		1.0 M KOH	51		264			[34]
$NiSe_2$/Ti	0.065 M $NiCl_2{\cdot}6H_2O$+ 0.035 M SeO_2+0.2 M LiCl	–0.45 V_{SCE} for 1 h	RT		1.0 M KOH	82		295			[35]
Ni_3Se_2-Au@Glass	10 mM $Ni(CH_3CO_2)_2{\cdot}4H_2O$+10 mM SeO_2 and 25 mM LiCl	–0.8 $V_{Ag/AgCl\ sat.}$ for 300 s	25	300 °C for 5 min under N_2	0.3 M KOH	97.1 97.2	310 290				[36]
NiP film	50 mM $NiCl_2$+1 M NaH_2PO_2+0.16 M glycine+0.1 M NaOAc	CV: 0.1~–1.1 $V_{Ag/AgCl\ sat.}$, scan rate of 50 mV/s, for 1 cycle (500 rpm)	-		1.0 M KOH	49	344		399		[37]
NiP/CF	1.3142 g $NiSO_4{\cdot}6H_2O$+ 0.4101 g NaOAc+ 2.1997 g NaH_2PO_2	CV: –1.0~–0.3 V_{SCE}, scan rate of 10 mV/s, for 15 cycles	-		1.0 M KOH	120	325				[38]
$N_{59}Cu_{19}P_9$	(45-49.9) mM $NiSO_4{\cdot}6H_2O$+(0.1-5) mM $CuSO_4{\cdot}5H_2O$+ 0.5 M NaH_2PO_2+ 0.15 M $C_2H_4(NH_2)_2$	Pulse: –8 mA for 1 s, –1.711 V_{SCE} until 20 C/cm^2 (1,500 rpm)	-		1.0 M KOH	42.5	307			0.006	[39]
CF@NiP_x	0.1 M Na_2SO_4+0.02 M Ni_2SO_4	–1.0 V_{SCE} for 5 min	-	300 °C for 120 min under Ar	1.0 M KOH	54.7	200			0.24	[40]
$NiFeP_x$-20/NF $NiFeP_x$-50/NF $NiFeP_x$-80/NF $NiFeP_x$-120/NF	(NiFe PBA/NF) 1 mM $K_3Fe(CN)_6$+ 1 mM $Ni(NO_3)_2{\cdot}6H_2O$+ 1 M $NaNO_3$	CV: 0-1 $V_{Ag/AgCl\ sat.}$, scan rate of 100 mV/s, for 20/50/80/120 min	-	350 °C for 2 hour under N_2	1.0 M KOH	44 43 29 33	239 226 224 233				[41]
NiCo-OH/ $Ni_2P_2O_7$	0.01 M $Ni(NO_3)_2{\cdot}6H_2O$+ $Co(NO_3)_2{\cdot}6H_2O$+DI water	–1.0 V_{SCE} for 300 s	-		1.0 M KOH	63	197		357		[42]

dec^{-1} in 1.0 M KOH electrolyte. In addition to the NiSe, NiP catalysts have also been actively investigated. For example, NiP catalysts fabricated by electrodeposition showed overpotential in the range of 320-350 mV at 10 mA cm^{-2} of OER current density [37, 38], which are competitive with those fabricated by chemical synthesis (290-500 mV at 10 mA cm^{-2}) [141,142]. In addition, Kim et al. prepared a NiCuP alloy catalyst using the electrodeposition and measured the OER activity in 0.1 M KOH electrolyte [39]. Their compound $Ni_{59}Cu_{19}P_9$ catalyst exhibited an overpotential of 307 mV at 10 mA cm^{-2} and Tafel slope of 42.5 mV dec^{-1}. XPS analysis showed that the addition of Cu metal to the NiP catalyst increased the amount of the Ni^{3+} species corresponding to NiOOH on the catalyst surface, thus improving the activity of the catalyst. In another investigation of Ni-based catalysts, Yuan et al. fabricated NiFe Prussian-blue analog (PBA) on Ni foam surfaces (PBA/NF) using the in-situ electrodeposition method and then prepared the NiFeP/NF catalyst through phosphidation process [41]. The $NiFeP_x$-80/NF catalyst (Figs. 3(a) and 3(b)) obtained using a deposition time of 80 min showed an overpotential of 224 mV at 10 mA cm^{-2} and Tafel slope of 29 mV dec^{-1} (Fig. 3(c)) in 1.0 M KOH electrolyte. The direct electrodeposition on conductive NF substrates obtained a microporous framework structure with an increased number of active sites, and the lack of the binder during electrodeposition also prevented the blockage of the active sites by the binder. Furthermore, the charge-transfer resistance measurements (Fig. 3(d)) supported the conclusion that the improvement in the OER activity was due to the enhanced electron transport.

1-2. Cu-based Electrocatalysts

Cu-based catalysts have the advantages of low cost, excellent electrical conductivity, and low toxicity compared to other transition metal-based catalysts (Ni, Co, Fe). Table 2 summarizes OER activity for the Cu-based and Co-based alloy catalysts prepared by the electrodeposition [49-51,58-62], with the Co-based alloy catalysts described in detail in Section 1-3. As Cu metal-based oxide catalysts have various oxidation states such as Cu^{+}, Cu^{2+}, and Cu^{3+}, they have been used in electrode applications such as lithium ion batteries [143,144] and photocatalysts [145,146]. It is known that the OER catalytic activity of transition metal oxides is governed by the d-orbital electronic structure because the bond formation and breaking during OER is associated with the bonding due to the interactions between the O-2p orbitals of the intermediate and the d-orbitals of the catalyst [147]. A representative work on an electrodeposited Cu-based OER catalyst was reported by Xu et al. [50]. They fabricated Cu_2O-Cu dendrites containing hybrid foam with a large surface area and good electronic conductivity to enhance the OER activity. The short diffusion path of the electrolyte and the fast transport of the active species led to the low onset overpotential of ~350 mV and low Tafel slope of 67.52 mV dec^{-1}. Chemically synthesized CuO catalysts with multi-walled carbon nanotubes, however, showed a relatively high overpotential of 420 mV at 10 mA cm^{-2} in 1.0 M KOH electrolyte [148]. A Cu-based compound catalyst with high activity and good chemical stability was reported by Deng et al. [51]. Using the electrodeposition-sulfurization method, they fabricated a $Cu_2S/TiO_2/Cu_2S$ catalyst for OER in 1.0 M KOH

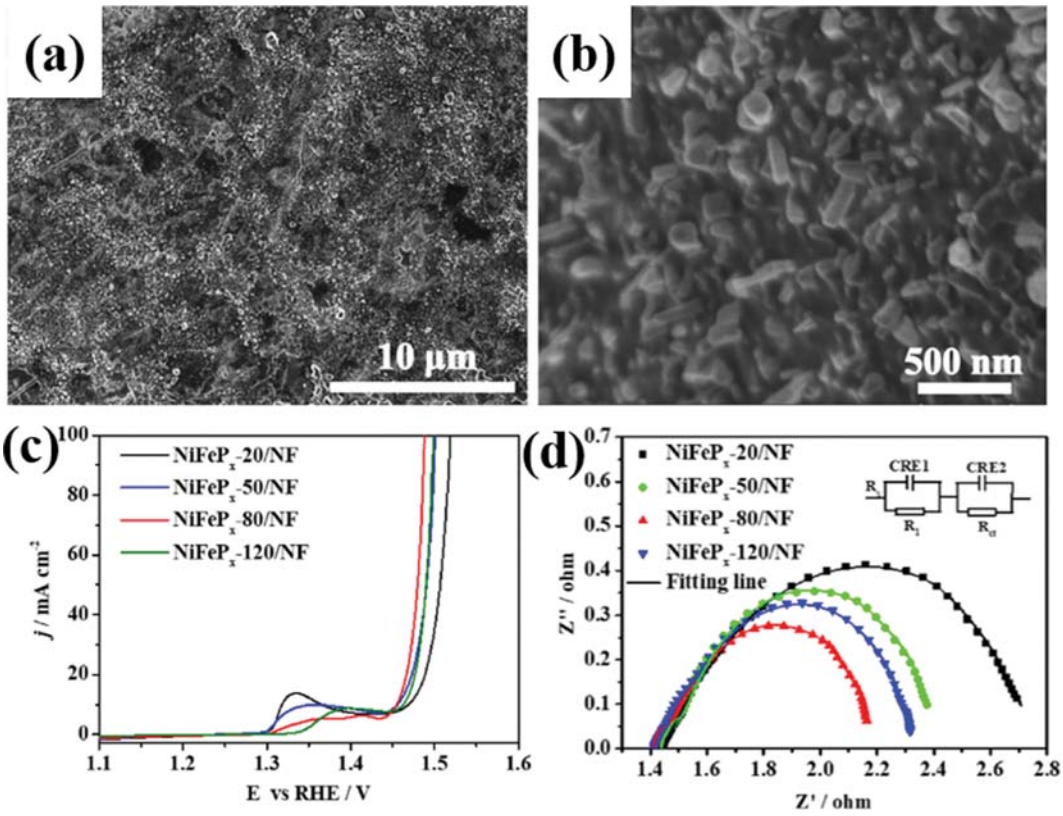

Fig. 3. (a), (b) SEM images of $NiFeP_x$-80/Ni foam (NF). (c) Polarization curves of $NiFeP_x$-20/NF, $NiFeP_x$-50/NF, and $NiFeP_x$-80/NF. (d) Electrochemical impedance spectra of $NiFeP_x$-80/NF (Reproduced with permission from Ref. [41] Copyright (2019) Elsevier).

Table 2. Summary of the alkaline OER performance for Cu- & Co-based catalysts

Catalyst	Deposition condition			Electrolyte	Tafel slope (mV dec^{-1})	Overpotential (mV)			Exchange current density (mA cm^{-2})	Ref.
	Electrolyte	Potential/Current/ Time	Temp. (°C)			η_{10}	η_{20}	η_{100}		
CuO NPs	0.2 mM $Cu(imidazole)_4Cl_2$+ MeCN/3% H_2O (v/v)+ 0.1 M $TBABF_4$	CV: –0.5~1.0 $V_{Ag/AgCl\ sat.}$, scan rate of 50 mV/s, for 2 cycles	-	1.0 M NaOH	64	290				[49]
Cu_2O-Cu foams	0.1 M $CuSO_4$+0.75 M H_2SO_4	3.6 A/cm^2 for 120 s	25	1.0 M KOH	67.52	350				[50]
Cu_2O foams	0.05 M $CuSO_4 \cdot 5H_2O$+ 0.5 M H_2SO_4	0.53 A/cm^2 for 5 min	25		77.25	387				
Cu foams	Reduction of Cu_2O-Cu foams by immersing in 1.5 M hydrazine hydrate	10 h	70		80.84	410				
$Cu_2S/TiO_2/Cu_2S$	(Anodic electrooxidation) Cu foam+1 M NaOH→ (ALD) $TiCl_4+H_2O$→ (Sulfurization) 0.1 M Na_2S	10 mA/cm^2 for 30 min →140 cycles→12 h	RT→ 120→90	1.0 M KOH	72	284				[51]
CoNi-OOH-30(40) nanosheet	1.5 mM $C_4H_6CoO_4 \cdot 4H_2O$+ 1.5 mM $NiCl_2 \cdot 6H_2O$+ 1.5 mM NH_4Cl+250 mL DI water→(electrooxidation) 1.0 M KOH	–10 mA/cm^2 for 30 min →50 mA/cm^2 for 40 h	-	1.0 M KOH	62	279				[58]
Electrodeposited CoS	0.05 M $CoSO_4$+0.2 M KSCN	–0.95 V_{SCE} for 1,200 s	-	1.0 M KOH	55	310				[59]
CoS/Ti mesh	5 mM $CoCl_2 \cdot 6H_2O$+0.75 M thiourea	CV: –1.2~0.2 $V_{Ag/AgCl\ sat.}$, scan rate of 5 mV/s, for 15 cycles	-	1.0 M KOH	64	361		430		[60]
CoP	50 mM $CoSO_4$+0.5 M NaH_2PO_2+0.1 M NaOAc	CV: –0.3~–1.0 $V_{Ag/AgCl\ sat.}$, scan rate of 5 mV/s, for 15 cycles (500 rpm)	-	1.0 M KOH	47	345		413		[61]
CoP-mesoporous nanorod arrays	25 mM $CoCl_2$+ 0.5 M NaH_2PO_2	–0.8 $V_{Ag/AgCl\ sat.}$	-	1.0 M KOH	65	300	309	362		[62]

electrolyte. The fabricated $Cu_2S/TiO_2/Cu_2S$ core-branch arrays exhibited 10-15 nm thick cross-linked Cu_2S branch nanoflakes, providing a large specific surface area and overflow of O_2; and a low overpotential (284 mV at 10 mA cm^{-2}) and small Tafel slope (72 mV dec^{-1}) were obtained for OER in an alkaline medium. This is similar to the activity of Cu_2S/Cu foam catalyst (an overpotential of 290 mV at 10 mA cm^{-2}) prepared by chemical synthesis [149].

1-3. Co-based Electrocatalysts

Similar to the Ni- and NiFe-based catalysts (Table 1), Co-based materials have attracted attention as potential catalysts for water electrolysis due to the excellent catalytic activity of the alloy [58], sulfides [59,60], and phosphides [61,62] of Co. Table 2 summarizes the OER activity for the Co-based catalysts. Potassium thiocyanate (KSCN) has been used in the fabrication of CoS because the dissociated SCN can form various complexes through the coordination of S or N atoms with transition metals [59,150]. Nan et al. reported a CoS catalyst on Ti foil fabricated by the electrodeposition method using KSCN [59]. The obtained electrodeposited CoS catalyst has a 3D flower-like nanostructure shape. This structure is beneficial for providing enriched active sites and an escape channel for the oxygen bubbles. While the electrodeposited Co catalysts in the absence of KSCN showed an overpotential of 480 mV at 10 mA cm^{-2} and Tafel slope of 99 mV dec^{-1}, the electrodeposited CoS catalyst exhibited higher OER activity with a lower overpotential of 310 mV at 10 mA cm^{-2} and Tafel slope of 55 mV dec^{-1}.

A substantial alkaline OER activity was also obtained using CoP catalysts by Zhu et al. [62]. They fabricated CoP-mesoporous nanorod arrays (MNA) catalysts with mesoporous nanorod array structures by the electrodeposition of a CoP catalyst on highly conductive Ni foams, rather than by using conventional phosphidation processes. The catalysts had a structure of uniformly grown vertically aligned nanorods with a diameter of 100 nm (Figs. 4(a)-(h)). These structural characteristics were advantageous for improving the electric interconnection and mass transport. In addition to the high activity for HER with an overpotential of 54 mV at 10 mA cm^{-2} and Tafel slope of 51 mV dec^{-1} (Fig. 4(i)), the catalyst showed good OER performance with an overpotential of 300 mV at 10 mA cm^{-2} and Tafel slope of 65 mV dec^{-1} (Fig. 4(j)). In addition, there was no substantial difference in the OER performances be-

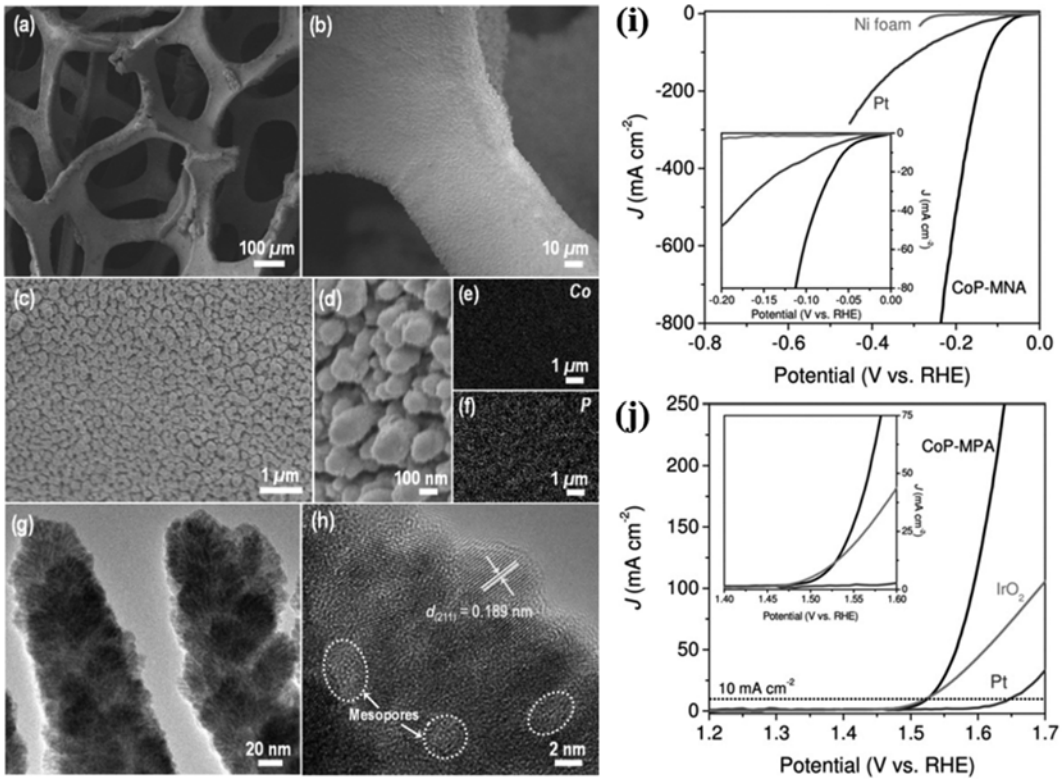

Fig. 4. (a)-(d) SEM, (e), (f) EDS elemental mapping, and (g), (h) TEM images of CoP-mesoporous nanorod arrays (MNA). (i) Polarization curves of CoP-MNA, Pt, and pristine Ni foam in H_2-saturated 1 M KOH aqueous solution at a scan rate of 2 mV s^{-1} (j) LSV polarization curves (2 mV s^{-1} in O_2-saturated 1 M KOH) of CoP-MNA, IrO_2, and Pt for electrocatalytic OER (Reproduced with permission from Ref. [62] Copyright (2015), Wiley).

tween CoP catalysts prepared either by electrodeposition (overpotential of 300 to 350 mV at 10 mA cm^{-2} [61,62]) or by chemical synthesis (overpotential of 310 to 360 mV at 10 mA cm^{-2} [69,151]).

2. Hydrogen Evolution Reaction (HER)

As is typically found in catalysis, electrocatalysts for HER require nanostructures with an appropriate hydrogen binding energy and also an improved surface-to-volume ratio necessary to obtain sufficient active sites for the reaction. Although Pt-based catalysts are known to show the best activity in alkaline HER, the high price and limited abundance of Pt hinder their use in practical applications [11]. Recently, research attention has been focused on the use of non-precious catalysts with a relatively high catalytic activity, low cost, and high stability obtained using alloys, compounds, and oxides of transition metals such as Cu, Fe, Ni, and Mo.

2-1. Ni-based Electrocatalysts

Ni-based catalysts have been studied as HER catalysts to replace Pt-based catalysts because Ni-based catalysts have relatively high activity and excellent resistance to corrosion in alkaline media and are more stable than other transition metals (e.g. Fe, Co) [34,35,37, 38,40,43-48,152,153]. Catalysts based on Ni alloys and Ni phosphides have been studied in order to improve the catalytic activity. Table 3 summarizes the HER activity for Ni-based alloy catalysts prepared by electrodeposition [34,35,37,38,40,43-46].

Gao et al. used a solution consisting of choline chloride-ethylene glycol eutectic solvent (ethaline) in a ratio of 1 : 2 to electrodeposit NiCu alloy catalysts with nanoporous structures arranged in nanosheets on Cu substrates [43]. In an evaluation of the HER activity in 1.0 M KOH electrolyte, nanoporous NiCu-3 alloy catalysts showed a low onset potential of 48 mV (overpotential of 128 mV at 10 mA cm^{-2}) and Tafel slope of 57.2 mV dec^{-1}.

In addition to NiCu, NiCo alloys are also known to be efficient for HER under alkaline conditions because of their improved intrinsic catalyst activity and corrosion resistance compared to pure Ni [43,45,152,154,155]. Preparation of nanostructured catalysts with an increased number of active sites and the fabrication of porous structures in order to increase the mass transport and electrical conductivity have been the typical strategies for obtaining NiCo alloy catalysts. Sun et al. fabricated a mesoporous NiCo alloy catalyst using electroless deposition and measured the HER activity of the obtained catalyst in alkaline media [45]. As shown in Figs. 5(a)-(f), NiCo catalysts with various lyotropic liquid crystal compositions were fabricated by the electroless deposition method. Among these, the mesoporous $Ni_{58}Co_{42}$ catalyst with a narrow pore size distribution of 3-5 nm showed the lowest onset overpotential of 52 mV (overpotential of 162 mV at 10 mA cm^{-2}) and Tafel slope of 60 mV dec^{-1} for HER (Fig. 5(g)). This result shows that a synergistic combination of Ni and Co, enlarged exposure of the catalytically active sites, and improved mass and charge transport led to excellent HER activity (Fig. 5(h)). A slightly better activity of an overpotential of 156 mV at 10 mA cm^{-2} in a 1.0 M KOH electrolyte was reported for chemically synthesized NiCo catalyst with heat treatment [152].

Table 3. Summary of the alkaline HER performance for Ni-based catalysts

Catalyst	Deposition condition			Electrolyte	Tafel slope (mV dec^{-1})	Overpotential (mV)			Exchange current density (mA cm^{-2})	Ref.
	Electrolyte	Potential/Current/ Time	Temp. (°C)			η_{10}	η_{20}	η_{100}		
NiFe/NF	0.2 M $NiSO_4 \cdot 7H_2O$+0.2 M $FeSO_4 \cdot 7H_2O$	CV: −0.2~−1.4 V_{SCE}, scan rate of 50 mV/s, for 60 cycles	RT	1.0 M KOH	112	139				[34]
$NiSe_2$/Ti	0.065 M $NiCl_2 \cdot 6H_2O$+0.035 M SeO_2+0.2 M LiCl	−0.45 V_{SCE} for 1 h	RT	1.0 M KOH	82	96				[35]
NiP film	50 mM $NiCl_2$+1 M NaH_2PO_2+ 0.16 M glycine+0.1 M NaOAc	CV: 0.1~−1.1 $V_{Ag/AgCl\ sat.}$, scan rate of 50 mV/s, for 1 cycle (500 rpm)	-	1.0 M KOH	43	93				[37]
NiP/CF	1.3142 g $NiSO_4 \cdot 6H_2O$+0.4101 g NaOAc+2.1997 g NaH_2PO_2	CV: −1.0~−0.3 V_{SCE}, scan rate of 10 mV/s, for 15 cycles	-	1.0 M KOH	55	98				[38]
CF@NiP_x	0.1 M Na_2SO_4+0.02 M Ni_2SO_4	−1.0 V_{SCE} for 5 min	-	1.0 M KOH	48.3	118			0.24	[40]
NiCu-1.5	50 mL ethaline+0.50 M $NiCl_2 \cdot 6H_2O$+0.10 M $CuCl_2 \cdot 2H_2O$	1.5, 3, 5.4 C/cm^2	60	1.0 M KOH	81.6	180	204		0.062	[43]
NiCu-3					57.2	128	150		0.151	
NiCu-5.4					74.5	158	182		0.098	
NiW (90)	90 g dm^{-3} sodium citrate+40 g dm^{-3} Na_2WO_4+80 g dm^{-3} nickel sulfate+7 g dm^{-3} ammonium chloride	Pulse: 12 A/dm^2, 1 A/ dm^2 for duration 600 s (250 rpm, 5,000 Hz)	70	1.0 M KOH	200	307	377			[44]
NiW (90-A)					130	169	226			
$Ni_{72}Co_{28}$	55 wt% Brij 58+(0-0.01) M $NiCl_2 \cdot 6H_2O$+(0-0.01) M $CoCl_2 \cdot 6H_2O$+2.2 g DI water→(Reduction) 0.6 g DMAB	Electroless deposition	80→RT	1.0 M NaOH	60	198				[45]
$Ni_{58}Co_{42}$					60	162				
$Ni_{51}Co_{49}$					81	213				
$Ni_{18}Co_{82}$					90	319				
PDD_Ni-10P	10 mM NaH_2PO_2+100 mM $NiCl_2 \cdot 6H_2O$	CV: −0.3~−1.0 $V_{Ag/Ag+}$, scan rate of 15 mV/s, for 50 cycles	60	1.0 M KOH	44.7	105				[46]
PSD_Ni-10P		−0.8 $V_{Ag/Ag+}$ (total 4.25 C/cm^2)			56.6	107				

In addition to alloying Ni with other transition metals, Ni phosphides have been shown to be beneficial for changing the electronic structure of the catalyst to lower the energy barrier to hydrogen adsorption, thus improving the HER activity [156]. Ledendecker et al. reported an Ni_5P_4 film catalyst fabricated by chemical synthesis with an HER overpotential of 150 mV at 10 mA cm^{-2} and Tafel slope of 53 mV dec^{-1} [153]. In contrast, Sun et al. fabricated a NiP catalyst using the methods of potentiostatic deposition (PSD) and potentiodynamic deposition (PDD) on Cu foil, and then compared the HER activity of the obtained catalysts in a 0.1 M KOH solution [46]. Figs. 6(a) and 6(b) show the SEM results of the catalysts prepared using the PSD and PDD methods, where the PDD-prepared catalysts exhibit a crack-free NiP_x film structure. For various NaH_2PO_2 concentrations in the electrolyte, NiP catalyst prepared with 10 mM NaH_2PO_2 concentration showed the best HER activity (overpotential of 105 mV at 10 mA cm^{-2} and Tafel slope of 44.7 mV dec^{-1}) (Fig. 6(c)). In addition, a negligible degradation of the catalytic activity was observed up to 1,000 cycles in stability testing (Fig. 6(d)). Fig. 6(e) shows the results of DFT calculations that found the water dissociation energy barrier (ΔG_{H2O}) of the P-doped Ni catalyst was substantially reduced to 0.34 eV, compared to that of the pure Ni metal (0.98 eV).

2-2. Co-based Electrocatalysts

For Co-based catalysts, many studies have been reported since it was found that phosphide-coupled Co catalysts exhibit excellent electrocatalytic HER activity. Table 4 summarizes the HER activity for the Co-based alloy catalysts prepared by electrodeposition [58,61-66]. Bai et al. fabricated a Co/CoP-Ni foam (NF) catalyst by the electrodeposition method and measured the HER activity in a 1.0 M NaOH solution [64], where NF with a large surface area due to the three-dimensional network structure played an important role in improving the catalytic activity. The subsequently electrode-

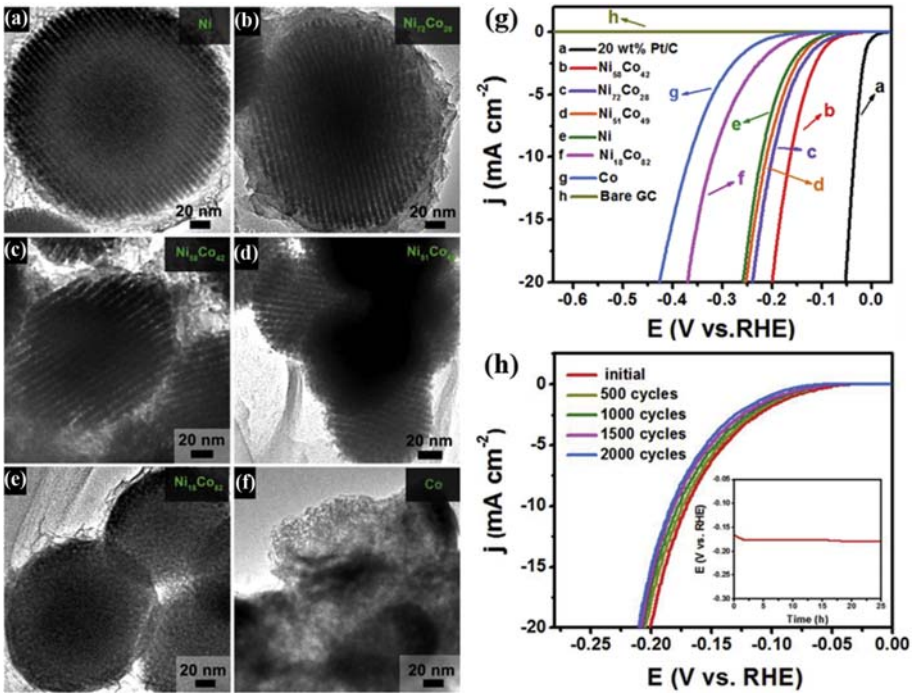

Fig. 5. TEM images of the mesostructured $Ni_{100-x}Co_x$ alloys prepared from different LLC (lyotropic liquid crystals) compositions: (a) Ni, (b) $Ni_{72}Co_{28}$, (c) $Ni_{58}Co_{42}$, (d) $Ni_{51}Co_{49}$, (e) $Ni_{18}Co_{82}$, and (f) Co. (g) Polarization curves for the HER on a bare glassy carbon (GC) electrode and modified GC electrodes comprising the mesoporous $Ni_{100-x}Co_x$ alloys in 1.0 M NaOH solution at a scan rate of 2 mV s^{-1}. (h) Polarization curves of the mesoporous $Ni_{58}Co_{42}$ alloy in 1.0 M NaOH solution initially and after 500, 1,000, 1,500, and 2,000 CV sweeps between −0.3 and +0.2 V vs. RHE, inset: time-dependent catalytic overpotential curve for mesoporous $Ni_{58}Co_{42}$ alloy at a static current density of −10 mA cm^{-2} for 25 h (Reproduced with permission from Ref. [45] Copyright (2017) Elsevier).

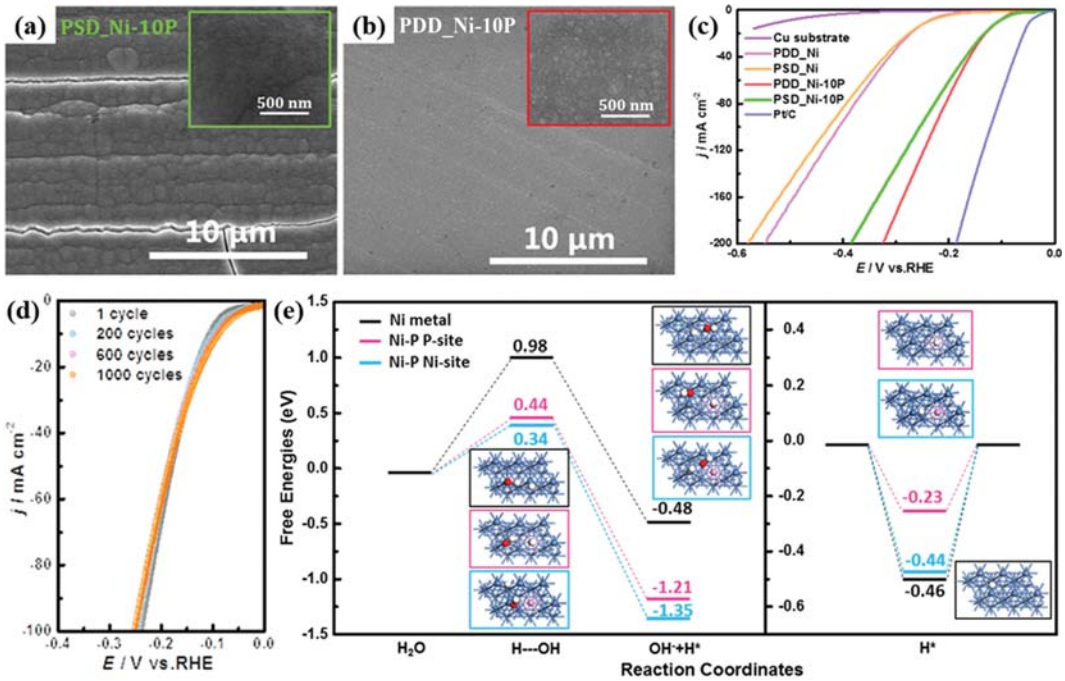

Fig. 6. SEM images of (a) potentiostatic deposition (PSD)_Ni-10P and (b) potentiodynamic deposition (PDD)_Ni-10P at different magnifications. (c) Polarization curves of commercial Pt/C catalyst, Cu foil, PDD_Ni, PSD_Ni, PDD_Ni-10P, and PSD_Ni-10P at a scan rate of 5 mV s^{-1} in 1 M KOH without IR correction. (d) Polarization curves of PDD_Ni-10P before and after 200, 600, and 1,000 CV cycles at a scan rate of 100 mV s^{-1} between −0.20 and 0.20 V vs. RHE. (e) Calculated adsorption free energy diagram of the alkaline HER (Volmer and Tafel processes) on the pure Ni metal and P-incorporated Ni sample with P- and Ni-sites (Reproduced with permission from Ref. [46] Copyright (2019) American Chemical Society).

Table 4. Summary of the alkaline HER performance for Co-based catalysts

Catalyst	Deposition condition			Electrolyte	Tafel slope (mV dec^{-1})	Overpotential (mV)			Exchange current density (mA cm^{-2})	Ref.
	Electrolyte	Potential/Current/ Time	Temp. (°C)			η_{10}	η_{20}	η_{100}		
CoNi-OOH-30(40) nanosheet	1.5 mM $C_4H_6CoO_4 \cdot 4H_2O$+ 1.5 mM $NiCl_2 \cdot 6H_2O$+ 1.5 mM NH_4Cl+ 250 mL DI water→ (electrooxidation) 1.0 M KOH	−10 mA/cm^2 for 30 min →50 mA/cm^2 for 40 h	-	1.0 M KOH	67	210				[58]
Co-P	50 mM $CoSO_4$+0.5 M NaH_2PO_2+0.1 M NaOAc	CV: −0.3~−1.0 $V_{Ag/AgCl\ sat.}$, scan rate of 5 mV/s, for 15 cycles (500 rpm)	-	1.0 M KOH	42	94				[61]
CoP-mesoporous nanorod arrays	25 mM $CoCl_2$+0.5 M NaH_2PO_2	−0.8 $V_{Ag/AgCl\ sat.}$	-	1.0 M KOH	51	54		121	0.857	[62]
$Co_{0.7}Mo_{0.3}P$	35 mM $Co(NO_3)_2$+25 mM $MoCl_5$+0.5 M NaH_2PO_2+ 0.1 M NaOAc	−1.4 $V_{Ag/AgCl\ sat.}$ for 600 s	-	1.0 M KOH	63	30				[63]
Co/CoP-NF	5 mM $CoSO_4 \cdot 7H_2O$+ 25 mM $NaH_2PO_2 \cdot H_2O$+ 5 mM CH_3COONa	−0.5 A/cm^2 for 10 min	RT	1.0 M KOH	71	35		130	3.10	[64]
$Co_2P/CoMoP_x$-0.4/NF	0.02 M $CoSO_4 \cdot 7H_2O$+ 0.05 M $Na_2MoO_4 \cdot 2H_2O$+ 0.9 M $NaH_2PO_2 \cdot H_2O$+ 0.12 M $C_6H_8O_7 \cdot H_2O$+ 0.18 M Na_2SO_4	−0.4 A/cm^2 for 5 min	RT	1.0 M NaOH	87.2	22		121	5.89	[65]
$Co(OH)_2$/CP	6 mM $Co(NO_3)_2$	2 mA/cm^2 for 20 min	RT	1.0 M KOH	236	406.8				[66]

posited Co/CoP catalyst on NF had a 3D network structure with low interfacial resistance and rapid release of bubbles generated on the electrode surface, giving an overpotential of 35 mV at 10 mA cm^{-2} and a Tafel slope of 71 mV dec^{-1}.

Similarly, Chen et al. measured the HER activity in the presence of 1.0 M NaOH after fabricating the crystalline/amorphous Co_2P/$CoMoP_x$ catalyst on NF [65]. By varying the deposition current density, they found that the $Co_2P/CoMoP_x$-0.4/NF catalyst electrodeposited at −0.4 A cm^{-2} showed a low overpotential of 22 mV at 10 mA cm^{-2} and Tafel slope of 87.2 mV dec^{-1}. Furthermore, the 50-hour stability test also showed good electrochemical stability. In the case of the CoP catalyst prepared by chemical synthesis [157, 158], they showed similar HER performance to that prepared by the electrodeposition. As an example, $CoP@CoO_x$ catalyst reported by Feng et al. [158] had the HER performance of an overpotential of 35 mV at 10 mA cm^{-2} and Tafel slope of 44.9 mV dec^{-1}.

PROTON EXCHANGE MEMBRANE WATER ELECTROLYSIS

1. Oxygen Evolution Reaction (OER): Ru- and Ir-based Electrocatalysts

Acidic OER operates in harsh electrochemical oxidative conditions compared to alkaline OER, requiring the use of noble metal-based oxide catalysts with high corrosion resistance against acidic environment [1,2,5,28-30]. Generally, two methods have been used for the fabrication of oxide catalysts. The first method is the production of thermal oxides using a heat treatment under an O_2 atmosphere. The second method is the production of defective electrochemical oxides using electrooxidation by applying anodic potentials (Figs. 7(a) and 7(b)) [31]. Danilovic et al. fabricated both thermal oxides and electrochemical oxides of Au, Pt, Ir, Ru, and Os and compared their OER performance and durability [31]. It was found that the OER activity increased with increasing oxygen-metal bond strength (oxophilicity) in the order of Au≪Pt<Ir<Ru≪Os [31,159]. On the other hand, durability showed the reverse order, that is, Os≪Ru<Ir<Pt≪Au, implying that a trade-off between the performance and durability is necessary, with the presence of defects playing an important role in the relationship between performance and durability (Fig. 7(a)) [31]. As indicated earlier, Ru oxide is known to have the second-highest activity for OER after Os oxide, but it suffers from extreme corrosion at high anodic potential, giving rise to problematic durability. Therefore, many studies have focused on improving the durability of Ru catalysts. For example, Kim et al. prepared Ru oxides by the sequential electrodeposition of Ru metal followed by thermal oxidation. The optimized heat treatment condition was determined by comparing the activity and durability for OER. Specifically, Ru oxide/Ti catalysts were produced by applying −0.6 V_{SCE} for 5 min on a Ti substrate using an electrolyte composed of 0.01 M $RuCl_3 \cdot xH_2O$+0.10 M HCl, fol-

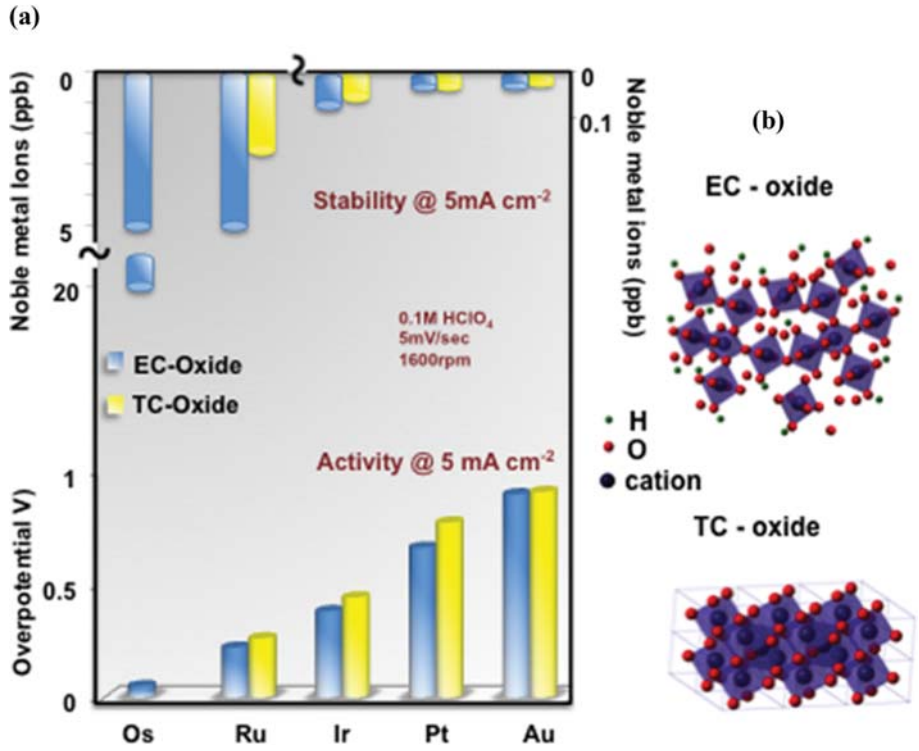

Fig. 7. Relationships between the activity and stability of the OER on monometallic oxides. (a) Inverse trends in activity and stability of the oxide materials prepared by the thermal chemical (TC) and electrochemical (EC) methods; (i) more noble materials are less active but more stable and (ii) because amorphous EC-oxides contain more defects, they are more active but less stable than the corresponding crystalline TC-oxides. (b) Schematic representation of the crystalline rutile TC-oxide and amorphous EC-oxide structures (Reproduced with permission from Ref. [31] Copyright (2014) American Chemical Society).

lowed by heat treatments at 300, 450, and 600 °C for 1 h under air conditions. Ru metal showed an excellent performance of 20 mA cm^{-2} at approximately 1.43 V_{RHE} but showed substantial deterioration due to dissolution after 10 cycles. On the other hand, Ru oxide produced by heat treatment at 450 °C showed negligible initial performance but showed the highest performance after 40 cycles of activation and maintained durability for 250 cycles [137]. In a follow-up study, a Ru/Co oxide catalyst was fabricated by the sequential electrodeposition of Co on a Ti substrate, followed by Ru electrodeposition. The electron transfer from Co to Ru and the morphology effect of the Co used as a sublayer improved the catalyst's performance from 16.2 mA cm^{-2} to 61 mA cm^{-2} at 1.64 V_{RHE}; however, durability was insufficient when the performance degraded by approximately 45.5% after 500 cycles [138]. Similar performance with the electrodeposition-fabricated Ru-based catalysts was reported by Tariq et al. [160] and Pascuzzi et al. [161], where the former was RuO_2/MoO_3 produced by hydrothermal method (1.49 V_{RHE} at 10 mA cm^{-2}) and the latter was Mn-TiO_2-RuO_2 fabricated by sol-gel method (1.616 V_{RHE} at 10 mA cm^{-2}), respectively.

Studies were also conducted on Ir oxide catalysts with moderate performance and excellent durability. Because of the low abundance and very high cost of Ir compared to Ru, research on Ir oxide catalysts has focused on reducing the catalyst content. Lee et al. electrodeposited IrO_2 on carbon paper and analyzed the changes in the loading amounts with the variation in the electrodeposition time and potential to determine the optimal electrodeposition conditions for application of the catalyst as a PEWME anode. The electrodeposition solution was composed of 10 mM $IrCl_4 \cdot H_2O$, 5 g L^{-1} of $(COOH)_2 \cdot 2H_2O$, and 10 g L^{-1} of 35% H_2O_2 in deionized water with sequential mixing of each component for the designated time. Then, K_2CO_3 was added to adjust the pH of the solution to 10.5, and the solution was prepared by stabilizing for three days. Afterwards, the electrodeposition time was varied from 1 to 30 min, and the deposition potential was adjusted from 0.6 to 0.9 V_{SCE}. It was found that the IrO_2 produced at 0.7 V_{SCE} for 10 min showed optimal PEMWE performance of 1.01 A cm^{-2} at 1.6 V_{cell} with a small loading of 0.1 mg cm^{-2}; these performance characteristics were superior to those of other IrO_2 catalysts produced by spraying, brushing, decal, and sputtering, demonstrating the advantages of electrodeposition as a catalyst fabrication technique [162]. Results are summarized in Table 5.

2. Hydrogen Evolution Reaction (HER)

Similar to alkaline HER, PGM catalysts that are known to have the highest activity and durability in acidic HER need to be replaced for large-scale hydrogen production because of their high price and limited reserves [1,2]. Therefore, studies have been conducted to develop an inexpensive material with sufficient activity and durability in order to replace Pt. Since HER operates at a relatively negative potential (reducing condition), it is possible to use non-PGM catalysts. Among them, Ni, Co, Fe, Mo, W, and Cu have been studied as potential materials [99]. However, as the single-metal catalysts have intrinsically low catalytic activity due to the inappropriate

Table 5. Summary of the acidic OER performance for Ru- & Ir-based catalysts

Catalyst	Deposition condition			Heat treatment	Electrolyte	Tafel slope (mV dec^{-1})	Overpotential (mV)			Exchange current density (mA cm^{-2})	Ref.
	Electrolyte	Potential/Current/ Time	Temp. (°C)				η_{10}	η_{20}	η_{100}		
Ru/Ti (1^{st})	0.01 M $RuCl_3$+ 0.10 M HCl	−0.6 V_{SCE} for 300 s	RT	-	0.5 M H_2SO_4	-	183	198	223	-	[137]
Ru/Ti450 (40^{th})	0.01 M $RuCl_3$+ 0.10 M HCl	−0.6 V_{SCE} for 300 s	RT	450 °C for 60 min under air	0.5 M H_2SO_4	-	258	293	-	-	
Ru/Co240/Ti	Ru: 0.02 M $RuCl_3$+ 0.10 M HCl/Co: 0.10 M $CoCl_2$+ 0.10 M HCl	Ru: −0.6 V_{SCE} for 300 s/Co: −1.0 V_{SCE} for 240 s	RT	375 °C for 60 min under air	0.5 M H_2SO_4	-	239	281	-	-	[138]
IrO_2	10 mM $IrCl_4 \cdot H_2O$+ 5 g/L $(COOH)_2 \cdot 2H_2O$+10 g/L 35% H_2O_2+K_2CO_3, pH 10.5	0.7 V_{SCE} for 10 min	-	-	0.1 M $HClO_4$	-	-	-	-	-	[162]

Table 6. Summary of the acidic HER performance for metal alloy catalysts

Catalyst	Deposition condition			Electrolyte	Tafel slope (mV dec^{-1})	Overpotential (mV)			Exchange current density (mA cm^{-2})	Ref.
	Electrolyte	Potential/Current/ Time	Temp. (°C)			η_{10}	η_{20}	η_{100}		
Ni_{100}	300 g/L $NiSO_4 \cdot 6H_2O$+50 g/L $NiCl_2 \cdot 6H_2O$+40 g/L H_3BO_3+ 1 g/L Sodium lauryl sulfate, pH 3.4	1,600 A/m^2 for 20 min	-	0.5 M H_2SO_4	147, 119	502			0.0026	[71]
$Ni_{77}W_{23}$	80 g/L $NiSO_4 \cdot 6H_2O$+50 g/L Potassium citrate+Excess Na_2CO_3+20 g/L $Na_2WO_4 \cdot 2H_2O$, pH 10.5	100 A/m^2 for 30 min	-	0.5 M H_2SO_4	43, 116	148			0.0103	
$Ni_{88}Mo_{12}$	79 g/L $NiSO_4 \cdot 6H_2O$+48 g/L $Na_2MoO_4 \cdot 2H_2O$+88 g/L Sodium citrate+Excess NH_4OH, pH 10.5	1,600 A/m^2 for 20 min	-	0.5 M H_2SO_4	38, 118	102			0.0205	
$Ni_{75}Mo_{25}$	52 g/L $NiSO_4 \cdot 6H_2O$+73 g/L $Na_2MoO_4 \cdot 2H_2O$+88 g/L Sodium citrate+Excess NH_4OH, pH 10.5	1,600 A/m^2 for 20 min	-	0.5 M H_2SO_4	40, 123	124			0.0124	
$Ni_{80}Fe_{20}$	80 g/L $NiSO_4 \cdot 6H_2O$+20 g/L $FeSO_4 \cdot 7H_2O$+50 g/L Sodium citrate+ 20 g/L Na_2CO_3+ H_2SO_4, pH 3.5	130 A/m^2 for 15 min	-	0.5 M H_2SO_4	94, 160	385			0.002	
$Ni_{15}Fe_{85}$	26 g/L $NiSO_4 \cdot 6H_2O$+28 g/L $FeSO_4 \cdot 7H_2O$+12 g/L H_3BO_3+ 3.6 g/L Na_2SO_4+H_2SO_4, pH 3	130 A/m^2 for 15 min	-	0.5 M H_2SO_4	86, 146	397			0.0004	
Ni_2Mo/PANI	NiMo: 52.1 g/L $NiSO_4 \cdot 6H_2O$+ 72.9 g/L $Na_2MoO_4 \cdot 2H_2O$+ 88 g/L $Na_3C_6H_5O_7 \cdot 2H_2O$+ Excess NH_4OH, pH 10.4/ PANI: 0.05 M Aniline+0.5 M H_2SO_4	NiMo: −1.45 V_{SCE} for 5 min/ PANI: 0.82 V_{SCE} for 5 min	-	0.5 M H_2SO_4	40	151			0.0054	[72]

Table 6. Continued

Catalyst	Deposition condition			Electrolyte	Tafel slope (mV dec^{-1})	Overpotential (mV)			Exchange current density (mA cm^{-2})	Ref.
	Electrolyte	Potential/Current/ Time	Temp. (°C)			η_{10}	η_{20}	η_{100}		
Ni_6Mo/PANI	NiMo: 79 g/L $NiSO_4 \cdot 6H_2O$+ 48 g/L $Na_2MoO_4 \cdot 2H_2O$+ 88 g/L $Na_3C_6H_5O_7 \cdot 2H_2O$+ Excess NH_4OH, pH 10.4/ PANI: 0.05 M Aniline+0.5 M H_2SO_4	NiMo: −1.45 V_{SCE} for 5 min/ PANI: 0.82 V_{SCE} for 5 min	-	0.5 M H_2SO_4	55	208			0.0112	[72]
Electrodeposited Ni	300 g/L $NiSO_4 \cdot 6H_2O$+50 g/L $NiCl_2 \cdot 6H_2O$+40 g/L H_3BO_3+ 1 g/L $Na_3C_{12}H_{25}SO_4 \cdot 2H_2O$	−70 mA/cm^2 for 1 min	55	0.5 M H_2SO_4	178				0.31	
$Ni_{85}Mo_{15}$	79 g/L $NiSO_4 \cdot 6H_2O$+48 g/L $Na_2MoO_4 \cdot 2H_2O$+88 g/L $Na_3C_6H_5O_7 \cdot 2H_2O$+Excess NH_4OH, pH 10.5	−70 mA/cm^2 for 1 min	55	0.5 M H_2SO_4	50, 138	76			3.63	[73]
$Ni_{1.6}Mo$/CF/CP	NiMo: 0.3 M $NiSO_4 \cdot 6H_2O$+ 0.2 M $Na_2MoO_4 \cdot 2H_2O$+ 0.3 M trisodium citrate dihydrate+0.03 M NaOH/ Cu foam: 0.12 M $CuSO_4 \cdot 5H_2O$+0.7 M H_2SO_4+1.2 M $(NH_4)_2SO_4$+0.4 mM 1,2,3-benzotriazole	NiMo: −1.4 V_{SCE} for 300 s/Cu foam: −0.3 A/ cm^2 for 1 s, −1.7 A/cm^2 for 5 s	RT	0.5 M H_2SO_4	96	68.7	98			[74]
$Ni_{50}Co_{50}$	0.084 M $NiSO_4 \cdot 7H_2O$+0.017 M $CoSO_4 \cdot 7H_2O$+0.1 M Sodium gluconate+10 g/L H_3BO_3+ 0.18 mM Cysteine, pH 4	5 A/dm^2 for 1 h	20 (293 K)	0.5 M H_2SO_4		328	368	616		[75]
$Ni_{51}Cu_{49}$	0.0935 M $NiSO_4 \cdot 7H_2O$+ 0.0065 M $CuSO_4 \cdot 5H_2O$+ 0.1 M Sodium gluconate+ 10 g/L H_3BO_3+0.18 mM Cysteine, pH 4.1	2.5 A/dm^2 for 1 h	20 (293 K)	0.5 M H_2SO_4		248	280	450		[76]
$Zn_{90.5}Ni_{9.5}$	0.01 M $ZnSO_4 \cdot H_2O$+0.09 M $NiSO_4 \cdot 7H_2O$+0.1 M Sodium gluconate+10 g/L H_3BO_3+ 0.18 mM Cysteine, pH 4	4 A/dm^2 for 30 min	20 (293 K)	0.5 M H_2SO_4	67.9	244	257	399		[77]
$Ni_{99}W_1$	45 mM tungstic acid+60 mM Na_2SO_3+52 mM Citric acid+ 125 mM $NiSO_4 \cdot 6H_2O$+ Ammonia, pH 9.9	−1.2 V for 300 s		0.5 M H_2SO_4	122	205	279			[78]
$Ni_{96}W_4$/CuNW/CP	NiW: 0.13 M $NiSO_4 \cdot 6H_2O$+ 0.12 M $Na_2WO_4 \cdot 2H_2O$+ 0.25 M $Na_3C_6H_5O_7$+0.1 M H_2SO_4	−1.6 V_{SCE} for 600 s	RT	0.5 M H_2SO_4	40	56	79	181		[79]
NiMoZn	40 mM $NiCl_2 \cdot 6H_2O$+20 mM Na_2MoO_4+0.2 mM $ZnCl_2$+ 0.13 M $Na_4P_2O_7$+0.89 M $NaHCO_3$+18.5 mM formic acid	120 mA/cm^2 for 10 min		0.5 M H_2SO_4	40	38	40			[80]

H bonding energy, researchers have focused on alloy or compound catalysts in order to improve the catalytic activity by adjusting the electronic structure of these elements or by increasing the number of active sites [81,82,163]. Although the same strategies are usually pursued for the development of alkaline and acidic HER catalysts, the results obtained for alkaline HER cannot be directly

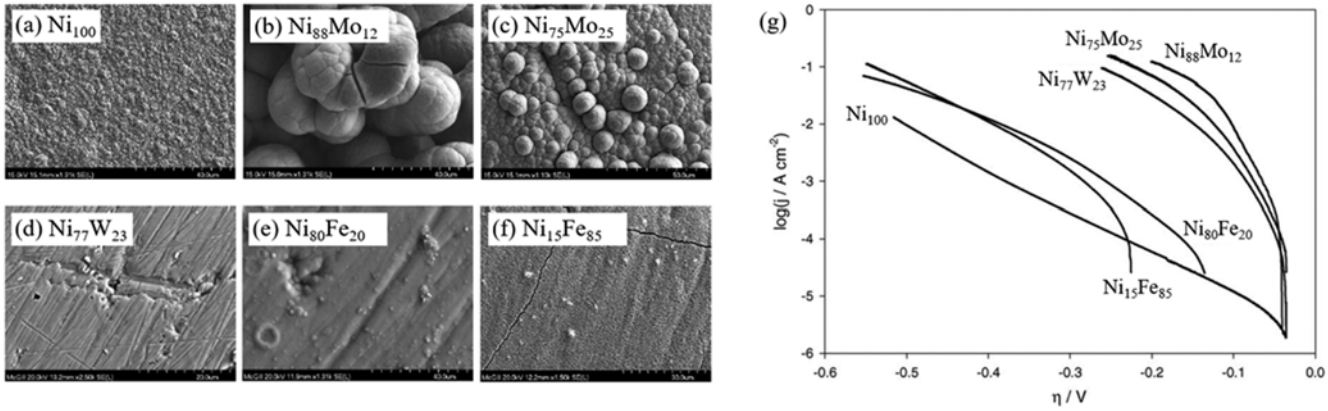

Fig. 8. (a)-(f) SEM images showing the surface morphology of electrodeposited NiX (X=Mo, W, Fe) coatings, (g) Tafel polarization curves recorded on NiX coatings in 0.5 M H_2SO_4 at 295 K. The scan rate was 0.5 mVs^{-1} (Reproduced with permission from Ref. [71] Copyright (2005) Elsevier).

applied to HER in PEMWE that operate at low pH and corrosive environments.

2-1. Metal Alloy Electrocatalysts

The electrodeposition conditions for the preparation of various metal catalysts and their HER performance characteristics are summarized in Table 6. In 2005, Navarro-Flores et al. reported various NiM (M=Mo, W, Fe) catalysts fabricated by electrodeposition with a constant current [71]. They controlled the concentrations of the Ni and M precursors in the electrolyte and applied a constant deposition current of 10-160 mA cm^{-2} for 15-30 min to fabricate catalysts with the compositions of Ni_{100}, $Ni_{88}Mo_{12}$, $Ni_{75}Mo_{25}$, $Ni_{77}W_{23}$, $Ni_{80}Fe_{20}$, and $Ni_{15}Fe_{85}$ on a Cu substrate. The results of the surface analysis conducted by FE-SEM and performance evaluation for HER are shown in Fig. 8. The addition of foreign metals to Ni resulted both in an increase in the electrochemical surface area and a simultaneous synergistic effect of electronic structure modification, giving rise to enhanced intrinsic activity. As a result, the $Ni_{88}Mo_{12}$ catalyst exhibited the best geometric activity with an overpotential of approximately 102 mV at 10 mA cm^{-2}, while $Ni_{77}W_{23}$ showed the highest intrinsic activity. The overpotential at 10 mA cm^{-2} of NiM was in the order of $Ni_{88}Mo_{12}$ (102 mV)<$Ni_{75}Mo_{25}$ (124 mV)<$Ni_{77}W_{23}$ (148 mV)<$Ni_{80}Fe_{20}$ (385 mV)<$Ni_{15}Fe_{85}$ (397 mV)< Ni (502 mV) (Fig. 8(g)).

In the same group, Damian et al. developed NiMo/PANI by sequential electrodeposition of a three-dimensional polyaniline (PANI) matrix, followed by NiMo deposition on the matrix to fabricate NiMo catalysts with a quasi-3D morphology. Among these catalysts, the Ni_2Mo/PANI catalyst showed the highest activity with an overpotential of approximately 151 mV at 10 mA cm^{-2} and a low Tafel slope of 40 mV dec^{-1}, while Ni_6Mo/PANI with high Ni content showed lower performance with an overpotential of approximately 208 mV; thus, these results showed a different tendency from their previous results of higher activity obtained for the higher Ni content [72]. They explained that this discrepancy is due to the increased surface area of Ni_2Mo/PANI that was approximately 5.9-times higher than that of Ni_6Mo/PANI, indicating the importance of the surface area effect on HER. Similarly, Martinez et al. developed a $Ni_{85}Mo_{15}$ catalyst with a porous structure using the constant current deposition method that showed a high catalytic activity with an overpotential of approximately 76 mV at 10 mA cm^{-2} and Tafel slope of 50 mV dec^{-1} [73]. Recently, in order to maximize the surface area of the catalyst, Kim et al. fabricated Cu foam (CF) on carbon paper (CP) using dynamic bubble-template electrodeposition [136], and $Ni_{1.6}Mo$/CF/CP with a high surface area was obtained by electrodepositing NiMo on the CF/CP [74]. The HER performance of this catalyst was significantly increased, obtaining an overpotential of 68.7 mV at 10 mA cm^{-2} and Tafel slope of 96 mV dec^{-1}. In addition to performing a half-cell evaluation, they used $Ni_{1.6}Mo$/CF/CP as the cathode in PEMWE and conducted a single-cell evaluation, demonstrating the feasibility of this catalyst for commercial use. Besides the electrodeposition, two-steps of the precipitation/reduction process were also investigated in the fabrication of NiMo nanopowders [164]. The fabricated catalyst exhibited excellent performance with an overvoltage of 70 mV at 20 mA cm^{-2}, but the catalyst rapidly deteriorated after the stability test at 20 mA cm^{-2} for 7 hrs.

In addition to the NiMo catalysts, Badawy and Nady et al. fabricated nanocrystalline NiCo, NiCu, and NiZn catalysts with optimized compositions to obtain the best HER performance characteristics (Fig. 9) [75-77]. The atomic composition of the catalyst was easily controlled by simply changing the concentration of the metal precursors in the electrodeposition bath. Badawy reported that the addition of Co to Ni led to valley-like morphology of NiCo catalysts with increased surface area [75]. The synergistic effect of the combination of Ni and Co gradually decreased the cathodic HER overpotential, resulting in the highest performance at 50.38 at% Co with an overpotential of approximately 328 mV at 10 mA cm^{-2} (Fig. 9(a)) and the highest corrosion resistance. For NiCu prepared by adding Cu to Ni, the best performance of an overpotential of 248 mV at 10 mA cm^{-2} and high durability was obtained for the $Ni_{51}Cu_{49}$ catalyst. This was attributed to the increased surface area due to the porous structure of the catalyst (Fig. 9(b)) [76]. They also reported the fabrication of a NiZn catalyst with increased surface area due to the coral reef-like and granular structures arising from the hydrogen generation during the co-deposition of Zn and Ni [77]. The addition of Zn changed the Ni d-band, resulting

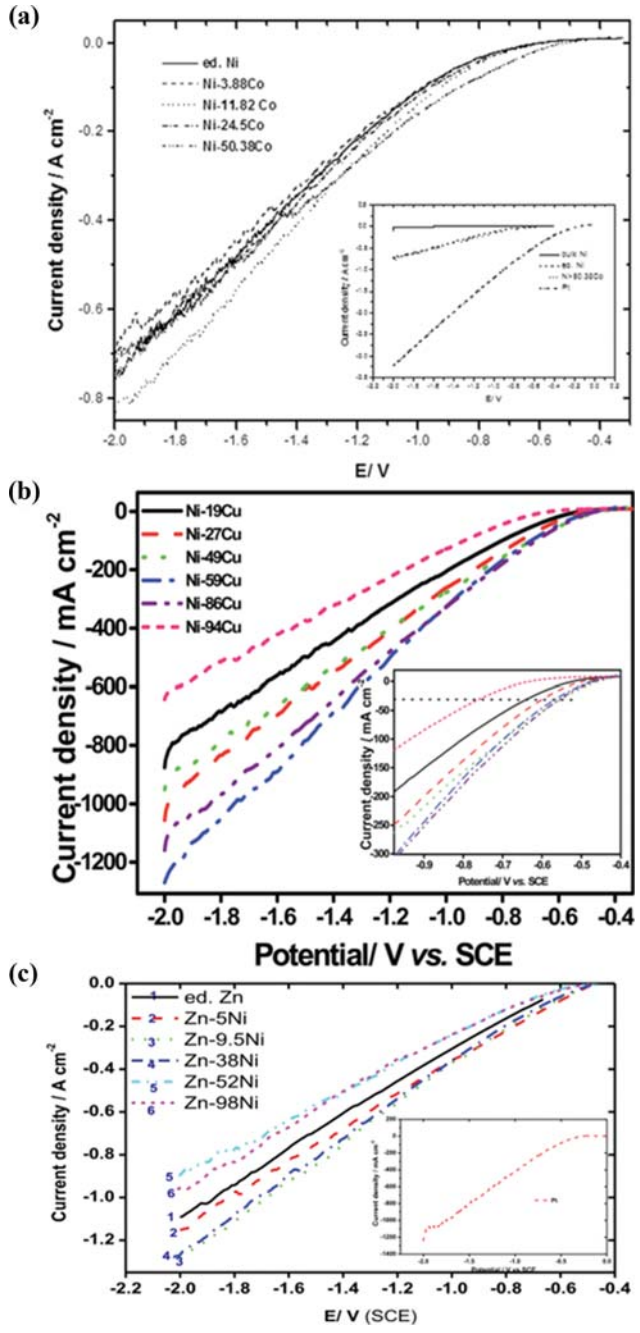

Fig. 9. Cathodic polarization of electrodeposited (a) NiCo, (b) NiCu, (c) NiZn catalysts in 0.5 M H_2SO_4 solutions at 25 °C (scan rate: 5 mV s^{-1}) (Reproduced with permission from Ref. [75-77] Copyright (2014, 2016, 2018) Elsevier).

in optimal performance for the $Ni_{9.5}Zn_{90.5}$ catalyst with an overpotential of approximately 244 mV at 10 mA cm^{-2} (Fig. 9(c)).

Tungsten is another candidate metal for Ni-based alloy catalysts. Bahari Mollamahale et al. reported spherical $Ni_{99}W_1$ NPs with the size of 100-200 nm [78]. The W content in their NiW catalysts was very low compared to other reports in the literature because they used FTO with a low conductivity as the substrate. HER activity evaluation found that the overpotential at 10 mA cm^{-2} was decreased by approximately 100 mV when pure Ni was alloyed with W. Furthermore, Kim et al. adopted both strategies of the optimization of the NiW composition and increase in the number of the active sites by using highly porous Cu nanowires (Cu NW) as a sublayer of the NiW catalyst [79]. They modulated the Ni/W atomic ratio by simply controlling the concentration of the Ni and W precursors in the electrolyte. As the electrodeposition rate was dependent on the concentration of the Ni precursor, the morphology of the underlying Cu NW sublayer was effectively maintained under low concentrations of the Ni precursor. In particular, $Ni_{96}W_4$/Cu NW/CP showed the highest performance with an overpotential of 56 mV at 10 mA cm^{-2} and Tafel slope of 40 mV dec^{-1}. Durability experiments showed that the performance reduction after long-term operation was due to the dissolution of Ni, NiO, and W. Similar WNi/Ni foam catalyst prepared by hydrothermal/annealing method was once reported by Nsanzimana et al. [165] of which the performance was somewhat low (an overvoltage of 100 mV at 10 mA cm^{-2}). However, the stability evaluations of the catalyst through repeating 1,000 cycles and applying 10 mA cm^{-2} for 12 hours suggested the feasibility of the catalyst.

In addition to the above-mentioned binary alloys, Wang et al. developed ternary NiMoZn alloy catalysts [80]. The NiMoZn ternary alloy catalysts with various compositions were electrodeposited on a Ni foil by controlling the concentrations of Ni and Zn in the electrodeposition bath. The HER performance was evaluated after activation through potential cycling (0~−0.4 V vs. Ag/AgCl (3 M KCl), 50 mV s^{-1}). The NiMoZn alloys with low Zn content (<3 at%) showed improved catalytic activity compared to NiMo, while the current density decreased and the overpotential increased as the content of Zn increased to ≥5 at%. The performance varication was reported to be closely related to the change in the oxidation states of the metallic Ni and Mo into Ni^{2+} and Mo^{n+} with increasing Zn content, as confirmed by the XPS analysis. Among the NiMoZn catalysts, the $Ni_{48.8}Mo_{49.2}Zn_2$ catalyst exhibited high performance with an overpotential of approximately 38 mV at 10 mA cm^{-2} and Tafel slope of approximately 40 mV dec^{-1} and also showed excellent durability even after 1,000 cycles.

2-2. Metal Compound Electrocatalysts

As non-metals have generally higher electronegativity than transition metals, they attract electrons from the transition metals, providing favorable electronic structure features for both the non-metal component and the electron-donating metal component and resulting in a synergistic effect that improves the HER performance [81, 82]. Accordingly, studies on the catalysts such as metal sulfides and phosphides have been actively conducted [81-92]. The electrodeposition conditions for the preparation of various metal compound catalysts and their HER performance characteristics are summarized in Table 7.

Merki et al. prepared amorphous MoS_x on an FTO substrate through potential cycling in the range of 0.3 to −0.8 V_{SHE}, using a 2 mM $(NH_4)_2MoS_4$ solution as the source of both Mo and S [83]. The HER performance evaluation in 1 M H_2SO_4 solution showed current density of 14 mA cm^{-2} and 160 mA cm^{-2} at the overpotentials of 200 mV and 300 mV, respectively. To overcome the low activity with the limited active sites of the 2D substrate, Min et al. used a three-dimensional (3D) Cu foam as the substrate and developed a 3D Cu foam@MoS_x catalyst by repeated cycling at a scan

Table 7. Summary of the acidic HER performance for metal compound catalysts

Catalyst	Deposition condition			Electrolyte	Tafel slope (mV dec^{-1})	Overpotential (mV)			Exchange current density (mA cm^{-2})	Ref.
	Electrolyte	Potential/Current/ Time	Temp. (°C)			η_{10}	η_{20}	η_{100}		
MoS_x	2 mM $(NH_4)_2[MoS_4]$	CV: 0.3~−0.8 V_{SHE}, scan rate of 50 mV/s, for 25 cycles	RT	1.0 M H_2SO_4	40	198				[83]
MoS_x/Cu foam	2 mM $(NH_4)_2[MoS_4]$+ 0.1 M $NaClO_4$	CV: −1.2~0.058 $V_{Ag/AgCl\ sat.}$, scan rate of 25 mV/s, for 30 cycles		0.5 M H_2SO_4	43.6	210	223	263		[84]
G-WS_2	5 mM $(NH_4)_2[MoS_4]$+ 1 mg/mL GO	CV: −1.2~0.5 $V_{Ag/AgCl}$, scan rate of 30 mV/s, for 30 cycles		0.5 M H_2SO_4	67	307	362			[85]
MoWS/CC	2 mM $(NH_4)_2MoS_4$+ 1 mM $(NH_4)_2WS_4$	CV: −1.2~0.2 $V_{Ag/AgCl\ sat.}$, scan rate of 40 mV/s. for 30 cycles	RT	0.5 M H_2SO_4	54	198	223	386	0.0123	[86]
$CoMoS_x$/CC	0.1 mM $Co(NO_3)_2{\cdot}6H_2O$+ 0.2 mM $(NH_4)_2[MoS_4]$ in 0.1 M PBS, pH 7	−0.5 V_{SCE} for 2 h	RT	0.5 M H_2SO_4	70	100	125	180	0.32	[87]
$Ni_{78}P_{22}$	0.5 M $NaCl_2{\cdot}6H_2O$+0.5 M $NaH_2PO_2{\cdot}H_2O$+0.1 M NH_4Cl, pH 4.4	Pulse: −1.0 V_{SCE} for 10 ms, −0.4 V_{SCE} for 20 ms, for 30 min	RT	0.5 M H_2SO_4	40	105	117	156		[92]
CoP	0.15 M H_3BO_3+0.10 M NaCl+0.30 M $NaPO_2H_2$+ 0.2 M $CoCl_2$, pH 5.0	−1.2 V_{SCE} for 15 min		0.5 M H_2SO_4	50	85	99		0.2	[93]

rate of 25 mV s^{-1} in a potential range of −1.2-0.058 $V_{Ag/AgCl\ sat.}$ in a 2 mM $(NH_4)_2MoS_4$+0.1 M $NaClO_4$ solution [84]. The MoS_x catalyst deposited on a Cu foil exhibited high overpotential of 274 and 402 mV at 10 and 100 mA cm^{-2}, respectively, whereas Cu foam@ MoS_x showed improved overpotential values of 200 and 250 mV at the same current densities and a low Tafel slope of 43.6 mV dec^{-1}, as well as stable durability for 2,000 cycles and 10 h. They claimed that the improved performance was due to the accelerated electron transfer and the increased number of active sites due to the use of a highly conductive Cu foam as the sublayer. Zhang et al. added Co through co-electrodeposition to improve the low conductivity of MoS_x [87]. By controlling the deposition potential and time, the thickness and shape of the $CoMoS_x$ film could be easily adjusted, and thus optimal conditions were found. The addition of Co to MoS_x increased the surface area by a factor of approximately 5.95, and faster electron transfer at the interface between electrolyte and electrocatalyst was enabled, resulting in an excellent catalytic performance with an overpotential of 100 mV at 10 mA cm^{-2} and Tafel slope of 70 mV dec^{-1}.

Similar to MoS_x, Pu et al. produced highly conductive graphene film-confined WS_2 (G-WS_2) through repeated cyclic voltammetry with $(NH_4)_2WS_4$ and graphene oxide (GO) that showed a lower overpotential of 306 mV at 10 mA cm^{-2} than WS_2 (343 mV at 10 mA cm^{-2}) [85]. Moreover, Li et al. fabricated MoWS on a carbon cloth in a one-step electrodeposition process [86]. The optimal fabrication conditions for making active catalysts for HER were determined by adjusting the concentration of the precursors, the potential range, number of cycles, and scanning speed during the electrodeposition. The MoWS catalyst had an overpotential of 198 mV at 10 mA cm^{-2} and low Tafel slope of 54 mV dec^{-1}. In addition to the electrodeposited catalysts, MoS_x-based catalysts (MoS_2, CoS_2/MoS_2/RGO, MoS_2/WC/RGO) fabricated by other methods (chemical vapor deposition, hydrothermal method, solvothermal method, respectively) showed similar performance with overpotentials of 160-200 mV at 10 mA cm^{-2} and low Tafel slopes of 41 to 56 mV dec^{-1} [166-168].

In addition to the metal sulfide catalysts, metal phosphide catalysts have been actively studied. Based on density functional theory (DFT) calculations, Liu et al. asserted that the (001) plane of Ni_2P was as efficient as Pt for HER [88]. The P content in Ni-P has also been shown to play a critical role in determining the HER activity [89-91]. Kim et al. manufactured Ni-P catalysts with various compositions through dissolution or further deposition of Ni by pulse electrodeposition [92]. It was found that the $Ni_{78}P_{22}$ catalyst showed the lowest overpotential of 105 mV at 10 mA cm^{-2} (Fig. 10(a)) and good durability for 500 cycles (Fig. 10(b)). From the XPS analysis of the correlation between the ratio of $Ni^{\delta+}$ and $P^{\delta-}$ and the HER performance, $Ni_{78}P_{22}$ showed the highest ratio of $Ni^{\delta+}$ and $P^{\delta-}$, implying that this composition has the most enhanced proton affinity (Fig. 10(c)). Ni_5P_4 catalyst prepared by colloidal synthesis showed slightly lower performance with an overpotential of 118 mV at 10 mA cm^{-2} despite having a large amount of P [90], but NiP_2 catalyst with more P prepared by hydrothermal/phosphidation showed good stability and higher performance with an overpotential of 75 mV at 10 mA cm^{-2} [91]. Studies on the Co phosphide catalysts have also been conducted. Saadi et al. produced a CoP catalyst with a Co to P ratio of 20 : 1 using constant potential deposition, and the obtained catalysts showed excellent performance with an overpotential of 85 mV at 10 mA cm^{-2} [93]. After 24 h of durability testing, the overpotential was increased by 18 mV, showing excellent durability; however, the Co to P ratio was rapidly reduced to 1 : 1 due to the removal of the amorphous-oxide

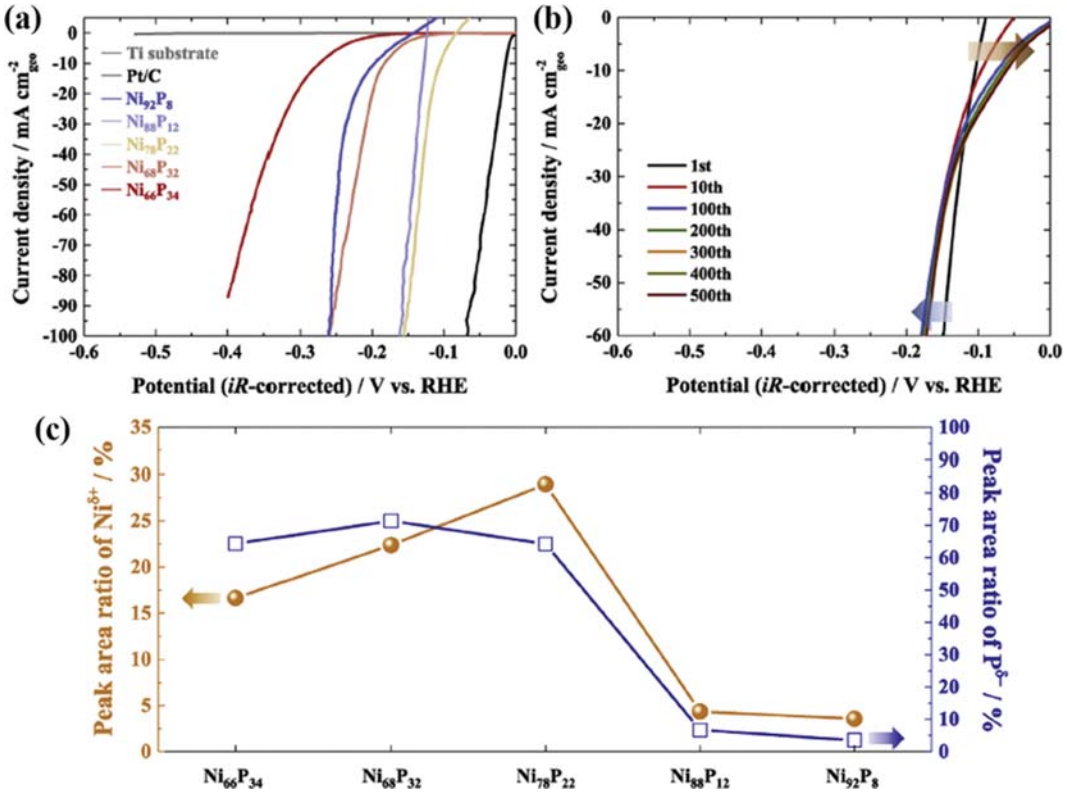

Fig. 10. (a) HER polarization curves of Ti substrate, Pt/C and NiP catalysts (scan rate: 5 mV s^{-1}), (b) accelerated degradation test of $Ni_{78}P_{22}$ up to 500th cycle (scan rate: 100 mV s^{-1}), (c) peak area ratio of $Ni^{\delta+}$ and $P^{\delta-}$ in NiP catalysts by XPS analysis (Reproduced with permission from Ref. [92] Copyright (2019) Elsevier).

during HER.

CONCLUSIONS

To date, noble-metal-based electrocatalysts have been mainly used in alkaline water electrolysis and proton exchange membrane water electrolysis systems to increase the energy efficiency of hydrogen production. In recent years, many studies have focused on the development of transition metal-based electrocatalysts with low cost and high performance for the replacement of the noble-metal-based electrocatalysts. In particular, the transition-metal-based electrocatalysts prepared by the electrodeposition method enable one-pot production of the catalyst-coated substrate (CCS) gas diffusion electrode in water electrolysis systems and exhibit a large number of electrochemically active sites and excellent catalytic activity. This review describes the material properties and catalytic activities of the electrodeposition-fabricated electrocatalysts applicable to the water electrolysis system, focusing on the non-noble metal-based catalysts, and suggests new strategies for the development of low-cost and high-activity water electrolysis catalysts using a simple and facile fabrication method.

ACKNOWLEDGEMENTS

This work was supported by the Hydrogen Energy Innovation Technology Development Program of the National Research Foundation (NRF) of Korea funded by Korean government (Ministry of Science and ICT (MSIT)) (grant number 2019M3E6A1063676). This work is also supported by the Chung-Ang University Research Scholarship Grants in 2020.

REFERENCES

1. M. Carmo, D. L. Fritz, J. Mergel and D. Stolten, *Int. J. Hydrogen Energy*, **38**, 4901 (2013).
2. S. S. Kumar and V. Himabindu, *Mater. Sci. Energy Technol.*, **2**, 442 (2019).
3. O. Schmidt, A. Gambhir, I. Staffell, A. Hawkes, J. Nelson and S. Few, *Int. J. Hydrogen Energy*, **42**, 30470 (2017).
4. P. Mocoteguy and A. Brisse, *Int. J. Hydrogen Energy*, **38**, 15887 (2013).
5. F. M. Sapountzi, J. M. Gracia, C. J. Weststrate, H. O. A. Fredriksson and J. W. Niemantsverdriet, *Prog. Energy Combust. Sci.*, **58**, 1 (2017).
6. C. Lamy, *Int. J. Hydrogen Energy*, **41**, 15415 (2016).
7. I. Vincent and D. Bessarabov, *Renew. Sustain. Energy Rev.*, **81**, 1690 (2018).
8. M. Gong, D.-Y. Wang, C.-C. Chen, B.-J. Hwang and H. Dai, *Nano Res.*, **9**, 28 (2016).
9. F. Yu, H. Zhou, Y. Huang, J. Sun, F. Qin, J. Bao, W. A. Goddardlll, S. Chen and Z. Ren, *Nat. Commun.*, **9**, 2551 (2018).
10. K. Zeng and D. Zhang, *Prog. Energy Combust. Sci.*, **36**, 307 (2010).
11. M. A. Khan, H. Zhao, W. Zou, Z. Chen, W. Cao, J. Fang, J. Xu, L.

Zhang and J. Zhang, *Electrochem. Energy Rev.*, **1**, 483 (2018).
12. A. N. Colli, H. H. Girault and A. Battistel, *Materials*, **12**, 1336 (2019).
13. A. H. A. Rahim, A. S. Tijani, S. K. Kamarudin and S. Hanapi, *J. Power Sources*, **309**, 56 (2016).
14. P. Nikolaidis and A. Poullikkas, *Renew. Sustain. Energy Rev.*, **67**, 597 (2017).
15. A. Skulimowska, M. Dupont, M. Zaton, S. Sunde, L. Merlo, D. J. Jones and J. Roziere, *Int. J. Hydrogen Energy*, **39**, 6307 (2014).
16. H.-J. Ban, M. Y. Kim, D. Kim, J. Lim, T. W. Kim, C. Jeong, Y.-A. Kim and H.-S. Kim, *J. Electrochem. Sci. Technol.*, **10**, 22 (2019).
17. F. Andolfatto, R. Durand, A. Michas, P. Millet and P. Stevens, *Int. J. Hydrogen Energy*, **19**, 421 (1994).
18. P. Millet, F. Andolfatto and R. Durand, *Int. J. Hydrogen Energy*, **21**, 87 (1996).
19. Y. Leng, G. Chen, A. J. Mendoza, T. B. Tighe, M. A. Hickner and C.-Y. Wang, *J. Am. Chem. Soc.*, **134**, 9054 (2012).
20. L. Xiao, S. Zhang, J. Pan, C. Yang, M. He, L. Zhuang and J. Lu, *Energy Environ. Sci.*, **5**, 7869 (2012).
21. S. Fiameni, I. Herraiz-Cardona, M. Musiani, V. Perez-Herranz, L. Vazquez-Gomez and E. Verlato, *Int. J. Hydrogen Energy*, **37**, 10507 (2012).
22. M. K. Kundu, T. Bhowmik, R. Mishra and S. Barman, *ChemSusChem*, **11**, 2388 (2018).
23. W. Luo. J. Gan, Z. Huang, W. Chen, G. Qian, X. Zhou and X. Duan, *Front. Mater.*, **6**, 251 (2019).
24. L. Zhang, K. Doyle-Davis and X. Sun, *Energy Environ. Sci.*, **12**, 492 (2019).
25. C. Li and J.-B. Baek, *ACS Omega*, **5**, 31 (2020).
26. S. A. Abbas, S.-H. Kim, M. I. Iqbal, S. Muhammad, W.-S. Yoon and K.-D. Jung, *Sci. Rep.*, **8**, 2986 (2018).
27. C. Chen, Y. Kang, Z. Huo, Z. Zhu, W. Huang, H. L. Xin, H. D. Snyder, D. Li, H. A. Herron, M. Mavrikakis, M. Chi, K. L. More, Y. Li, N. M. Markovic, G. A. Somorjai, P. Yang and V. R. Stamenkovic, *Science*, **343**, 1399 (2014).
28. R. Frydendal, E. A. Paoli, B. P. Knudsen, B. Wickman, P. Malacrida, I. E. L. Stephens and I. Chorkendorff, *ChemElectroChem*, **1**, 2075 (2014).
29. S. Park, Y. Shao, J. Liu and Y. Wang, *Energy Environ. Sci.*, **5**, 9331 (2012).
30. W. Hu, Y. Wang, X. Hu, Y. Zhou and S. Chen, *J. Mater. Chem.*, **22**, 6010 (2012).
31. N. Danilovic, R. Subbaraman, K.-C. Chang, S. H. Chang, Y. J. Kang, J. Snyder, A. P. Paulikas, D. Strmcnik, Y.-T. Kim, D. Myers, V. R. Stamenkovic and N. M. Markovic, *J. Phys. Chem. Lett.*, **5**, 2474 (2014).
32. X. Tan, J. Shen, N. Semagina and M. Secanell, *J. Catal.*, **371**, 57 (2019).
33. L.-K. Wu, Y.-X. Zhu, M. Liu, G.-Y. Hou, Y.-P. Tang, H.-Z. Cao, H.-B. Zhang and G.-Q. Zheng, *Int. J. Hydrogen Energy*, **44**, 5899 (2019).
34. Q. Luo, M. Peng, X. Sun, Y. Luo and A. M. Asiri, *Int. J. Hydrogen Energy*, **41**, 8785 (2016).
35. Z. Pu, Y. Luo, A. B. Asiri and X. Sun, *ACS Appl. Mater. Interfaces*, **8**, 4718 (2016).
36. A. T. Swesi, J. Masud and M. Nath, *Energy Environ. Sci.*, **9**, 1771 (2016).
37. N. Jiang, B. You, M. Sheng and Y. Sun, *ChemCatChem*, **8**, 106 (2016).
38. Q. Liu, S. Gu and C. M. Li, *J. Power Sources*, **299**, 342 (2015).
39. B. K. Kim, S.-K. Kim, S. K. Cho and J. J. Kim, *Appl. Catal. B-Environ.*, **237**, 409 (2018).
40. Z. Zang, S. Liu, J. Xiao and S. Wang, *J. Mater. Chem. A*, **4**, 9691 (2016).
41. B. Yuan, F. Sun, C. Li, W. Huang and Y. Lin, *Electrochim. Acta*, **313**, 91 (2019).
42. N. R. Chodankar, I. V. Bagal, S.-W. Ryu, Y.-K. Han and D.-H. Kim, *ChemCatChem*, **11**, 4256 (2019).
43. M. Y. Gao, C. Yang, Q. B. Zhang, Y. W. Yu, Y. X. Hua, Y. Li and P. Dong, *Electrochim. Acta*, **215**, 609 (2016).
44. P. J. Rad, M. Aliofkhazraei and G. B. Darband *Int. J. Hydrogen Energy*, **44**, 880 (2019).
45. T. Sun, J. Cao, J. Dong, H. Du, H. Zhang, J. Chen and L. Xu, *Int. J. Hydrogen Energy*, **42**, 6637 (2017).
46. C. Sun, J. Zeng, H. Lei, W. Yang and Q. Zhang, *ACS Sustain. Chem. Eng.*, **7**, 1529 (2019).
47. N. V. Krstajic, V. D. Jovic, L. Gajic-Krstajic, B. M. Jovic, A. L. Antozzi and G. N. Martelli, *Int. J. Hydrogen Energy*, **33**, 3676 (2008).
48. X. Yu, M. Wang, Z. Wang, X. Gong and Z. Guo, *Electrochim. Acta*, **211**, 900 (2016).
49. T. N. Huan, G. Rousse, S. Zanna, I. T. Lucas, X. Xu, N. Menguy, V. Mougel and M. Fontecave, *Angew. Chem. Int. Ed.*, **56**, 4792 (2017).
50. H. Xu, J.-X. Feng, Y.-X. Tong and G.-R. Li, *ACS Catal.*, **7**, 986 (2017).
51. S. Deng, Y. Shen, D. Xie, Y. Lu, X. Yu, L. Yang, X. Wang, X. Xia and J. Tu, *J. Energy Chem.*, **39**, 61 (2019).
52. C. Panda, P. W. Menezes, M. Zheng, S. Orthmann and M. Driess, *ACS Energy Lett.*, **4**, 747 (2019).
53. B. Zhang, C. Li, G. Yang, K. Huang, J. Wu, Z. Li, X. Cao, D. Peng, S. Hao and Y. Huang, *ACS Appl. Mater. Interfaces*, **10**, 23807 (2018).
54. P. Muthukumar, V. V. Kumar, G. R. K. Reddy, P. S. Kumar and S. P. Anthony, *Catal. Sci. Technol.*, **8**, 1414 (2018).
55. H. Zhang, Z. Zhang, N. Li, W. Yan and Z. Zhu, *J. Catal.*, **352**, 239 (2017).
56. C.-C. Hou, W.-F. Fu and Y. Chen, *ChemSusChem*, **9**, 2069 (2016).
57. B. Kumar, G. K. Rao, S. Saha and A. K. Ganguli, *ChemPhysChem*, **17**, 155 (2016).
58. C. Yu, J. Lu, L. Luo, F. Xu, P. K. Shen, P. Tsiakaras and S. Yin, *Electrochim. Acta*, **301**, 449 (2019).
59. K. Nan, H. Du, L. Su and C. M. Li, *ChemistrySelect*, **3**, 7081 (2018).
60. T. Liu, Y. Liang, Q. Liu, X. Sun, Y. He and A. M. Asiri, *Electrochem. Commun.*, **60**, 92 (2015).
61. N. Jiang, B. You, M. Sheng and Y. Sun, *Angew. Chem. Int. Ed.*, **54**, 6251 (2015).
62. Y.-P. Zhu, Y.-P. Liu, T.-Z. Ren and Z.-Y. Yuan, *Adv. Fun. Mater.*, **25**, 7337 (2015).
63. A. C. Themuwara, L. Dheer, N. H. Attanayake, Q. Yan, U. V. Waghmare and D. R. Strongin, *ChemCatChem*, **10**, 4832 (2018).
64. N. Bai, Q. Li, D. Mao, D. Li and H. Dong, *ACS Appl. Mater. Interfaces*, **8**, 29400 (2016).
65. X. Chen, Q. Li, Q. Che, Y. Chen and X. Xu, *ACS Sustain. Chem. Eng.*, **7**, 2437 (2019).
66. H. Wu, X. Zuo, S.-P. Wang, J.-W. Yin and Y.-N. Zhang, *Prog. Nat. Sci. Mater.*, **29**, 356 (2019).
67. J. A. Koza, Z. He, A. S. Miller and J. A. Switzer, *Chem. Mater.*, **24**, 3567 (2012).

68. K. Xu, H. Ding, M. Zhang, M. Chen, Z. Hao, L. Zhang, C. Wu and Y. Xie, *Adv. Mater.*, **29**, 1606980 (2017).
69. C.-Z. Yuan, S.-L. Zhong, Y.-F. Jiang, Z. K. Yang, Z.-W. Zhao, S.-J. Zhao, N. Jiang and A.-W. Xu, *J. Mater. Chem. A*, **5**, 10561 (2017).
70. P. Chen, K. Xu, Y. Tong, X. Li, S. Tao, Z. Fang, W. Chu, X. Wu and C. Wu, *Inorg. Chem. Front.*, **3**, 236 (2016).
71. E. Navarro-Flores, Z. Chong and S. Omanovic, *J. Mol. Catal. A-Chem.*, **226**, 179 (2005).
72. A. Damian and S. Omanovic, *J. Power Sources*, **158**, 464 (2006).
73. S. Martinez, M. Metikos-Hukovic and L. Valek, *J. Mol. Catal. A-Chem.*, **245**, 114 (2006).
74. J. H. Kim, J. Kim, H. Kim, J. Kim and S. H. Ahn, *J. Ind. Eng. Chem.*, **79**, 255 (2019).
75. W. A. Badawy, H. Nady and M. Negem, *Int. J. Hydrogen Energy*, **39**, 10824 (2014).
76. H. Nady and M. Negem, *RSC Adv.*, **6**, 51111 (2016).
77. H. Nady and M. Negem, *Int. J. Hydrogen Energy*, **43**, 4942 (2018).
78. Y. B. Mollamahale, N. Jafari and D. Hosseini, *Mater. Lett.*, **213**, 15 (2018).
79. H. Kim, H. Park, D.-K. Kim, S. Oh, I. Choi and S.-K. Kim, *ACS Sustain. Chem. Eng.*, **7**, 8265 (2019).
80. X. Wang, R. Su, H. Aslan, J. Kibsgaard, S. Wendt, L. Meng, M. Dong, Y. Huang and F. Besenbacher, *Nano Energy*, **12**, 9 (2015).
81. X. Zou and Y. Zhang, *Chem. Soc. Rev.*, **44**, 5148 (2015).
82. Y. Shi and B. Zhang, *Chem. Soc. Rev.*, **45**, 1529 (2016).
83. D. Merki, S. Fierro, H. Vrubel and X. Hu, *Chem. Sci.*, **2**, 1262 (2011).
84. S. Min, J. Qin, W. Hai, Y. Lei, J. Hou and F. Wang, *Int. J. Hydrogen Energy*, **43**, 4978 (2018).
85. Z. Pu, Q. Liu, A. M. Asiri, A. Y. Obaid and X. Sun, *Electrochim. Acta*, **134**, 8 (2014).
86. C. Li, X. Bo, M. Li and L. Guo, *Int. J. Hydrogen Energy*, **42**, 15479 (2017).
87. N. Zhang, W. Ma, F. Jia, T. Wu, D. Han and L. Niu, *Int. J. Hydrogen Energy*, **41**, 3811 (2016).
88. P. Liu and J. A. Rodriguez, *J. Am. Chem. Soc.*, **127**, 14871 (2005).
89. A. R. J. Kucernak and V. N. N. Sundaram, *J. Mater. Chem. A*, **2**, 17435 (2014).
90. Y. Pan, Y. Liu, J. Zhao, K. Yang, J. Liang, D. Liu, W. Hu, D. Liu, Y. Liu and C. Liu, *J. Mater. Chem. A*, **3**, 1656 (2015).
91. P. Jiang, Q. Liu and X. Sun, *Nanoscale*, **6**, 13440 (2014).
92. H. Kim, H. Park, D.-K. Kim, I. Choi and S.-K. Kim, *J. Alloys Compd.*, **785**, 296 (2019).
93. F. H. Saadi, A. I. Carim, E. Verlage, J. C. Hemminger, N. S. Lewis and M. P. Soriaga, *J. Phys. Chem. C*, **118**, 29294 (2014).
94. C. Hu, L. Zhang and J. Gong, *Energy Environ. Sci.*, **12**, 2620 (2019).
95. W. Sheng, H. A. Gasteiger and Y. Shao-Horn, *J. Electrochem. Soc.*, **157**, B1529 (2010).
96. N. M. Markovic, S. T. Sarraf, H. A. Gasteigert, J. Philip and N. Ross, *J. Chem. Soc., Faraday Trans.*, **92**, 3719 (1996).
97. E. Skulason, G. S. Karlberg, J. Rossmeisl, T. Bligaard, J. Greeley, H. Jonsson and J. K. Norskov, *Phys. Chem. Chem. Phys.*, **9**, 3241 (2007).
98. R. Gomez, A. Fernandez-Vega, J. M. Feliu and A. Aldaz, *J. Phys. Chem.*, **97**, 4769 (1993).
99. J. K. Norskov, T. Bligaard, A. Logadottir, J. R. Kitchin, J. G. Chen, S. Pandelov and U. Stimming, *J. Electrochem. Soc.*, **152**, J23 (2005).
100. W. Sheng, M. Myint, J. G. Chen and Y. Yan, *Energy Environ. Sci.*, **6**, 1509 (2013).
101. N.-T. Suen, S.-F. Hung, Q. Quan, N. Zhang, Y.-J. Xu and H. M. Chen, *Chem. Soc. Rev.*, **46**, 337 (2017).
102. B. Wang, X. Cui, J. Huang, R. Cao and Q. Zhang, *Chin. Chem. Lett.*, **29**, 1757 (2018).
103. X. Wang, A. Vasileff, Y. Jiao, Y. Zheng and S. Z. Qiao, *Adv. Mater.*, **31**, 1803625 (2019).
104. J. O. M. Bockris, *J. Chem. Phys.*, **24**, 817 (1956).
105. R. L. Doyle and M. E. G. Lyons, *J. Electrochem. Soc.*, **160**, H142 (2013).
106. T. Shinagawa, A. T. Garcia-Esparza and K. Takanabe, *Sci. Rep.*, **5**, 13801 (2015).
107. J. K. Norskov, J. Rossmeisl, A. Logadottir, L. Lindqvist, J. R. Kitchin, T. Bligaard and H. Jonsson, *J. Phys. Chem. B*, **108**, 17886 (2004).
108. A. Damjanovic, A. Dey and J. O. M. Bockris, *Electrochim. Acta*, **11**, 791 (1966).
109. J. Yu, Q. He, G. Yang, W. Zhou, Z. Shao and M. Ni, *ACS Catal.*, **9**, 9973 (2019).
110. Y. Yang, H. Fei, G. Ruan and J. M. Tour, *Adv. Mater.*, **27**, 3175 (2015).
111. J. Barber, *Chem. Soc. Rev.*, **38**, 185 (2009).
112. E. A. Paoli, F. Masini, R. Frydendal, D. Deiana, P. Malacrida, T. W. Hansen, I. Chorkendorff and I. E. L. Stephens, *Catal. Today*, **262**, 57 (2016).
113. Y. Pi, N. Zhang, S. Guo, J. Guo and X. Huang, *Nano Lett.*, **16**, 4424 (2016).
114. C. Spori, P. Briois, H. N. Nong, T. Reier, A. Billard, S. Kuhl, D. Teschner and P. Strasser, *ACS Catal.*, **9**, 6653 (2019).
115. E. Antolini, *ACS Catal.*, **4**, 1426 (2014).
116. S.-H. Jeon, W.-I. Choi, G.-D. Song, Y.-H. Son and D. H. Hur, *Coatings*, **6**, 62 (2016).
117. K.-S. Choi, *Dalton Trans.*, 5432 (2008).
118. L. Xu, Y. Guo, Q. Liao, J. Zhang and D. Xu, *J. Phys. Chem. B*, **109**, 13519 (2005).
119. S. H. Lee, H. Lee, M. S. Cho, J.-D. Nam and Y. Lee, *J. Mater. Chem. A*, **1**, 14606 (2013).
120. S. H. Hong, S. H. Ahn, I. Choi, S. G. Pyo, H.-J. Kim, J. H. Jang and S.-K. Kim, *Appl. Surf. Sci.*, **307**, 146 (2014).
121. J.-E. Lim, U. J. Lee, S. H. Ahn, E. Cho, H.-J. Kim, J. H. Jang, H. Son and S.-K. Kim, *Appl. Catal. B-Environ.*, **165**, 495 (2014).
122. S. H. Hong, S. H. Ahn, J. Choi, J. Y. Kim, H. Y. Kim, H.-J. Kim, J. H. Jang, H. Kim and S.-K. Kim, *Appl. Surf. Sci.*, **349**, 629 (2015).
123. J. Choi, M. J. Kim, S. H. Ahn, I. Choi, J. H. Jang, Y. S. Ham, J. J. Kim and S.-K. Kim, *Chem. Eng. J.*, **299**, 37 (2016).
124. H. Kim, E. Hwang, H. Park, B.-S. Lee, J. H. Jang, H.-J. Kim, S. H. Ahn and S.-K. Kim, *Appl. Catal. B-Environ.*, **206**, 608 (2017).
125. E. Hwang, H. Park, H. Kim, S. H. Ahn and S.-K. Kim, *Bull. Korean Chem. Soc.*, **38**, 607 (2017).
126. H. Park, J. Choi, H. Kim, E. Hwang, D.-H. Ha, S. H. Ahn and S.-K. Kim, *Appl. Catal. B-Environ.*, **219**, 123 (2017).
127. E. Hwang, H. Kim, H. Park, T. Lim, Y.-T. Kim, S. H. Ahn and S.-K. Kim, *J. Nanosci. Nanotechnol.*, **17**, 7547 (2017).
128. H. Park, H. Kim, E. Hwang, S. H. Ahn and S.-K. Kim, *J. Nanosci. Nanotechnol.*, **17**, 7843 (2017).
129. H. Kim, S. Choi, H. Park, J. H. Jang, S. H. Ahn and S.-K. Kim,

Nanoscale, **9**, 19045 (2017).
130. H. Park, S. Choe, H. Kim, D.-K. Kim, G. Cho, Y. Park, J. H. Jang, D.-H. Ha, S. H. Ahn and S.-K. Kim, *Appl. Surf. Sci.*, **444**, 303 (2018).
131. H. Park, K. M. Kim, H. Kim, D.-K. Kim, Y. S. Won and S.-K. Kim, *Korean J. Chem. Eng.*, **35**, 1547 (2018).
132. D.-K. Kim, H. Kim, H. Park, S. Oh, S. H. Ahn, H.-J. Kim and S.-K. Kim, *J. Power Sources*, **438**, 227022 (2019).
133. S. Oh, Y. S. Park, H. Park, H. Kim, J. H. Jang, I. Choi and S.-K. Kim, *J. Ind. Eng. Chem.*, **82**, 374 (2020).
134. H. Kim, H. Park, S. Oh and S.-K. Kim, *Int. J. Energy Res.*, **44**, 2833 (2020).
135. H. Park, D.-K. Kim, H. Kim, S. Oh, W. S. Jung and S.-K. Kim, *Appl. Surf. Sci.*, **510**, 145444 (2020).
136. Y. Li, W.-Z. Jia, Y.-Y. Song and X.-H. Xia, *Chem. Mater.*, **19**, 5758 (2007).
137. J. Y. Kim, J. Choi, H. Y. Kim, E. Hwang, H.-J. Kim, S. H. Ahn and S.-K. Kim, *Appl. Surf. Sci.*, **359**, 227 (2015).
138. J. Y. Kim, H. Park, H. Kim, E. Hwang, S. H. Ahn and S.-K. Kim, *Bull. Korean Chem. Soc.*, **37**, 1270 (2016).
139. A. Ganesan and M. Narayanasamy, *Mater. Renew. Sustain. Energy*, **8**, 18 (2019).
140. G.-R. Li, H. Xu, X.-F. Lu, J.-X. Feng, Y.-X. Tong and C.-Y. Su, *Nanoscale*, **5**, 4056 (2013).
141. L.-A. Stern, L. Feng, F. Song and X. Hu, *Energy Environ. Sci.*, **8**, 2347 (2015).
142. A. Han, H. Chen, Z. Sun, J. Xu and P. Du, *Chem. Commun.*, **51**, 11626 (2015).
143. P. Subalakshmi and A. Sivashanmugam, *J. Alloys Compd.*, **690**, 523 (2017).
144. Z. Wang, Y. Zhang, H. Xiong, C. Qin, W. Zhao and X. Liu, *Sci. Rep.*, **8**, 6530 (2018).
145. Q. Shi, G. Ping, Z. Wang, H. Xu, J. Li, J. Cui, H. Abroshan, H. Ding and G. Li, *J. Mater. Chem. A*, **7**, 2253 (2019).
146. N. D. Khiavi, R. Katal, S. K. Eshkalak, S. Masudy-Panah, S. Ramakrishna and H. Jiangyong, *Nano Mater.*, **9**, 1011 (2019).
147. Z. Zhou, X. Li, Q. Li, Y. Zhao and H. Pang, *Mater. Today Chem.*, **11**, 169 (2019).
148. M. Qian, X. Liu, S. Cui, H. Jia and P. Du, *Electrochim. Acta*, **263**, 318 (2018).
149. L. He, D. Zhou, Y. Lin, R. Ge, X. Hou, X. Sun and C. Zheng, *ACS Catal.*, **8**, 3859 (2018).
150. N. Wang, L. Li, D. Zhao, X. Kang, Z. Tang and S. Chen, *Small*, **13**, 1701025 (2017).
151. B. You, N. Jiang, M. Sheng, S. Gul, J. Yano and Y. Sun, *Chem. Mater.*, **27**, 7636 (2015).
152. B. Zhang, X. Zhang, Y. Wei, L. Xia, C. Pi, H. Song, Y. Zheng, B. Gao, J. Fu and P. K. Chu, *J. Alloys Compd.*, **797**, 1216 (2019).
153. M. Ledendecker, S. K. Calderon, C. Papp, H.-P. Steinruck, M. Antonietti and M. Shalom, *Angew. Chem. Int. Ed.*, **54**, 12361 (2015).
154. L. Yu, T. Lei, B. Nan, Y. Jiang, Y. He and C. T. Liu, *Energy*, **97**, 498 (2016).
155. S. Baranton and C. Coutanceau, *Appl. Catal. B-Environ.*, **136-137**, 1 (2013).
156. Y. Lu, Y. Deng, S. Lu, Y. Liu, J. Lang, X. Cao and H. Gu, *Nanoscale*, **11**, 21259 (2019).
157. J. Wang, W. Yang and J. Liu, *J. Mater. Chem. A*, **4**, 4686 (2016).
158. L. Fang, Y. Xie, Y. Yang, B. Zhu, Y. Wang, M. Liu, K. Zhao, H. Zhao and J. Zhang, *ACS Appl. Energy Mater.*, **3**, 309 (2020).
159. J. K. Norskov, J. Rossmeisl, A. Logadottir and L. Lindqvist, *J. Phys. Chem. B*, **108**, 17886 (2004).
160. M. Tariq, Y. Wu, C. Ma, M. Ali, W. Q. Zaman, Z. Abbas, K. S. Ayub, J. Zhou, G. Wang, L.-M. Cao and J. Yang, *Int. J. Hydrogen Energy*, **45**, 17287 (2020).
161. M. E. C. Pascuzzi, A. Goryachev, J. P. Hofmann and E. J. M. Hensen, *Appl. Catal. B-Environ.*, **261**, 118225 (2020).
162. B.-S. Lee, S. H. Ahn, H.-Y. Park, I. Choi, S. J. Yoo, H.-J. Kim, D. Henkensmeier, J. Y. Kim, S. Park, S. W. Nam, K.-Y. Lee and J. H. Jang, *Appl. Catal. B-Environ.*, **179**, 285 (2015).
163. Z. W. She, J. Kibsgaard, C. F. Dickens, I. Chorkendorff, J. K. Norskov and T. F. Jaramillo, *Science*, **355**, eaad4998 (2017).
164. J. R. McKone, B. F. Sadtler, C. A. Werlang, N. S. Lewis and H. B. Gray, *ACS Catal.*, **3**, 166 (2013).
165. J. M. V. Nsanzimana, Y. Peng, M. Miao, V. Reddu, W. Zhang, H. Wang, B. Y. Xia and X. Wang, *ACS Appl. Nano Mater.*, **1**, 1228 (2018).
166. M. A. Lukowski, A. S. Daniel, F. Meng, A. Forticaux, L. Li and S. Jin, *J. Am. Chem. Soc.*, **135**, 10274 (2013).
167. Y.-R. Liu, X. Shang, W.-K. Gao, B. Dong, J.-Q. Chi, X. Li, K.-L. Yan, Y.-M. Chai, Y.-Q. Liu and C.-G. Liu, *Appl. Surf. Sci.*, **412**, 138 (2017).
168. Y. Yan, B. Xia, X. Qi, H. Wang, R. Xu, J.-Y. Wang, H. Zhang and X. Wang, *Chem. Commun.*, **49**, 4884 (2013).

Soo-Kil Kim received his BS (1999), MS (2001), and Ph D (2004) degrees from School of Chemical and Biological Engineering, Seoul National University, Korea. From 2005 to 2006, he worked as a guest researcher at National Institute of Standards and Technology, Gaithersburg, USA. After that he joined Fuel Cell Research Center, Korea Institute of Science and Technology as a senior research scientist. In 2011, he joined School of Integrative Engineering, Chung-Ang University as a faculty member. He has published more than 130 papers and 58 international and domestic patents on electrocatalysts for fuel cell, CO_2 conversion, and water electrolysis as well as on metal interconnection for semiconductor devices. He has served in various positions at The Korean Institute of Chemical Engineers, The Korean Electrochemical Society, and The Electrochemical Society (USA).